JOURNAL OF GUIDANCE, CONTROL, AND DYNAMICS
Vol. 33, No. 4, July–August 2010

Design of Forcing Functions for the Identification of Human Control Behavior

H. J. Damveld,* G. C. Beerens,† M. M. van Paassen,‡ and M. Mulder§
Delft University of Technology, 2600 GB Delft, The Netherlands

DOI: 10.2514/1.47730

Human control behavior, as exercised during vehicle or aircraft control, can be identified by applying forcing functions with a specific frequency content to excite the human control system. The presence of these forcing functions may affect human control behavior as well, an effect which is not well-understood and might considerably affect the result of experiments. Common metrics, such as spectral shape and bandwidth, have been shown to be insufficient in predicting the forcing function's effect on human control behavior. This paper investigates the effect of forcing function phase on the control behavior, as well as the effect of the forcing function frequencies at which power is present, within a fixed spectral shape. These effects were tested in a human-in-the-loop compensatory tracking experiment. Our experiment showed that the effects of the frequencies were substantial. For this reason, a new metric was proposed to better predict the effects of forcing functions on the human control behavior, and to allow comparison between forcing functions with different spectral shapes and frequency contents. The metric considers the variance of the signal's derivatives. To test the validity of the metric, forcing functions with equal derivative variances were used in a compensatory tracking experiment. The outcome of the experiment reveals that the resulting behavior indeed can be considered equal when the variances are equal, even when the forcing function spectral shapes are considerably different.

Nomenclature

A_j	=	sinusoidal amplitude, in.
$e(t)$	=	tracking error, in.
K_c	=	controlled dynamics gain, in./in.
$n(t)$	=	operator remnant activity, deg
T	=	measurement time, s
$u(t)$	=	stick deflection, deg
$Y_c(j\omega)$	=	controlled element dynamics
$Y_{\text{ol}}(j\omega)$	=	open-loop describing function
$Y_p(j\omega)$	=	operator describing function
$y(t)$	=	system output, in.
ζ	=	damping ratio
ρ_a^2	=	squared relative remnant
σ_i	=	forcing function standard deviation, in.
τ_d	=	pure time delay, s
τ_e	=	effective time delay, s
τ_L	=	lead-time constant, s
τ_l	=	lag-time constant, s
$\Phi(\omega)$	=	power spectral density, in.^{2}s/rad
ϕ_j	=	sinusoidal phase, deg
φ_M	=	phase margin, deg
ω_c	=	gain crossover frequency, rad/s
ω_i	=	forcing function bandwidth, rad/s
ω_{nm}	=	neuromuscular bandwidth, rad/s

Presented as Paper 6026 at the AIAA Modeling and Simulation Technologies Conference, Chicago, IL, 10–13 August 2009; received 20 October 2009; revision received 1 February 2010; accepted for publication 5 February 2010.

*Postdoctoral Research Fellow, Control and Simulation Division, Faculty of Aerospace Engineering, P.O. Box 5058; H.J.Damveld@TUDelft.nl. Member AIAA.

†Researcher, Control and Simulation Division, Faculty of Aerospace Engineering, P.O. Box 5058; gijsbeerens@gmail.com.

‡Associate Professor, Control and Simulation Division, Faculty of Aerospace Engineering, P.O. Box 5058; M.M.vanPaassen@TUDelft.nl. Member AIAA.

§Professor, Control and Simulation Division, Faculty of Aerospace Engineering, P.O. Box 5058; M.Mulder@TUDelft.nl. Senior Member AIAA.

I. Introduction

IN THE application of system identification to describe the human controller in closed-loop tracking tasks, forcing function signals are used to excite the operator's control behavior [1–13]. Some studies [1–3,5] show that human operators may adapt their control strategy to the forcing function itself, however.

The design of forcing functions requires the experimenter to meet a number of objectives. The excitation signals should be fairly representative of the actual task. In addition, the excitation signals should be unpredictable for the human, and difficult enough to prevent boredom, in order to ensure high levels of control behavior linearity and limit between-subject variability [2,3]. Furthermore, the signals should not become too difficult to avoid excessive workload. In the extreme, a difficult forcing function could lead to adopting a lower tracking bandwidth to improve performance, a phenomenon commonly referred to as crossover regression [2,3,14].

The majority of forcing function variants found in the literature are sum-of-sinusoids with customized power spectra [2,5,6,9,10,15]. For a specific type of spectrum shape, the effect of the forcing function on control behavior is assumed to be fully determined by just one characteristic, bandwidth [2,3]. Recent experiments in our human–machine laboratory indicated that other aspects of the forcing function signal may affect human control behavior as well [5,6,14].

The fact that it is difficult to anticipate the effects of choosing a particular forcing function on human control behavior complicates the design of experiments. As more effects than crossover regression may occur [8–10], it is also unclear how to compare the results of two experiments that are in principle identical except for different forcing functions. Hence, there is a need for a more systematic approach to predict and experimentally control the effects of forcing functions on human control behavior.

This paper describes a new metric to make such a prediction. It is based on describing the forcing function using the variance of not only the forcing function signal itself but also those of the signal's derivatives. These variances of the derivatives weigh the forcing function power spectrum by frequency. Our main assumption is that when humans are presented with two forcing functions that are

different but comprise approximately the same variances, the resulting control behavior will be similar. In other words, through describing the forcing function by its variances, its effect on control behavior can be predicted reasonably well.

This paper is structured in two parts. First, common classes of forcing functions, as well as some generally accepted design principles, are reviewed. Then, in a theoretical analysis the equal-variances metric is proposed for analyzing and designing forcing functions. In addition, the effect of the phase realization of sum-of-sinusoids signals is investigated. Based on this analysis, a set of hypotheses is formulated. The second part of the paper describes the results of an experiment performed to test the hypotheses, designed after McRuer et al.'s [2] 1965 experiment. The paper concludes with the major findings on forcing function design and its effect on human control behavior as observed in the theoretical and experimental analysis.

II. Review of Forcing Function Design Principles

A. Forcing Function Definition and Requirements

Forcing functions are often composed as a sum-of-sinusoids [2] [see Eq. (1)]. Each sinusoid is defined by the frequency ω_j, the magnitude A_j, and the phase φ_j. In the process of designing a particular forcing function, each of these parameters must be addressed:

$$i(t) = \sum_{j=1}^{N} A_j \sin(\omega_j t + \varphi_j) \tag{1}$$

To describe human characteristics, McRuer et al. [2] studied control behavior in the frequency domain. A representation of a human operator performing a compensatory tracking task with a certain controlled element is shown in Fig. 1. The human pilot control characteristics are modeled by a system composed of a linear describing function Y_p and a remnant signal n, where the remnant represents the part of the measured response that the linear model cannot account for. Generally speaking, the more linear the human control behavior, the lower the remnant signal power.

To obtain accurate and adequate operator models, forcing functions must comply with four requirements:

1) The forcing function must be random-appearing, to prevent the human from detecting patterns in the signal. When the human controller can anticipate the forcing function, his behavior can no longer be modeled by a feedback system, but should include a feedforward path as well [2,13].

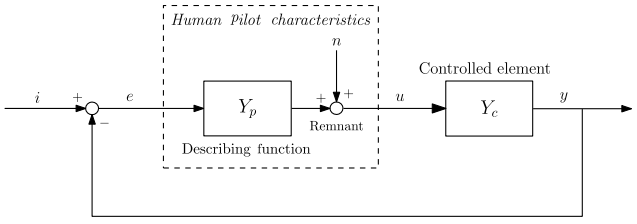

Fig. 1 Quasi-linear compensatory-operator model represented by a describing function plus remnant [2].

2) The forcing function must be sufficiently exciting, to get the human engaged in the proper way and maximize the accuracy of the describing function [2,3,5,14].

3) The forcing function must have a high signal-to-noise ratio at frequencies of interest, to maximize the accuracy of identification [3].

4) The forcing function must have a Gaussian magnitude distribution, to obtain describing functions that resemble real-life control behavior as closely as possible [13,14].

Frequency-domain identification requires high signal-to-noise ratios at a limited number of frequencies [2,3]. Time-domain identification has more relaxed requirements [16,17]. Two additional requirements for frequency-domain identification methods hold. First, the number of sinusoids is limited such that the signal power does not get diluted over too many frequencies. Second, preferably an equally spaced separation on a logarithmic scale of the integer frequencies over approximately two decades is applied in order to identify the describing function [2,3,13].

B. Examples of Forcing Function Spectra

Over the years, various types of forcing function spectra have been defined, some of which are illustrated in Fig. 2. The discrete step spectrum introduced by McRuer et al. [2], shown in Fig. 2a, has often been used in control behavior experiments [2,3,7,18–20]. Other discrete spectra, shown in Figs. 2b and 2c, were introduced in later attempts to improve the signal-to-noise ratios in the frequency range between the low- and high-magnitude sinusoids [5,9,10,15,16]. Continuous spectra (Fig. 2d) introduced in the pioneering work of Elkind [1] reappeared in the 1970s but were reported to suffer from low signal-to-noise ratios [8] and unexpected crossover-regression effects.

The forcing function bandwidth is defined as the frequency at which a significant drop can be seen in the magnitude in the spectral density plot. Three step-spectra forcing functions were defined by McRuer et al. [2], with 1.5, 2.5, and 4.0 rad/s bandwidth. In the remainder of this paper, we will refer to these forcing functions as the Systems Technology, Inc. (STI) 6-4, 7-3, and 8-2 forcing functions. The numbers refer to the number of high-magnitude and low-magnitude sinusoids. By assuming that the low-frequency, high-magnitude sinusoids account for the largest portion of the signal, only a marginal effect of the high-frequency, low-magnitude sinusoids on control behavior is assumed [2]. For this reason the bandwidth was generally considered to be the main factor affecting control behavior.

Bandwidth, however, might not be the only factor. During the setup of experiments in a number of studies [5,6,14] pilot comments and mean-squared error performance measures indicated that a forcing function with a low bandwidth was considered to be more difficult and resulted in a lower performance than identical forcing functions with a slightly higher bandwidth. On closer inspection the low-bandwidth forcing function appeared to be crested more heavily, resulting in higher velocities and accelerations. Cresting is performed by adjusting the phase of the individual sinusoidal components in the forcing function only. The traditional relation between mean-squared error and forcing function bandwidth was retained by using a low-bandwidth forcing function with a lower crest factor.

A similar phenomenon was observed when sinusoids were added to the forcing function just below the bandwidth. Although the total

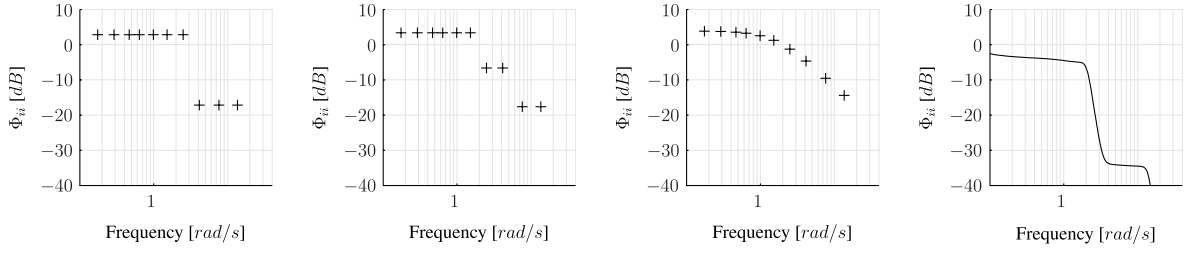

a) Step spectrum[2] **b) Multistep spectrum[6,13]** **c) Shaping filter[5,15,16]** **d) Continuous spectrum[8]**

Fig. 2 Some well-known forcing function spectra (all standardized to 0.5 in. standard deviation).

forcing function power and bandwidth remained equal, the performance and pilot comments changed.

These findings indicated that forcing function characteristics other than bandwidth affect the control behavior. An alternative approach developed in this paper is to more precisely characterize the various signal properties. When the human is presented signals with highly similar characteristics, control behavior can be expected to be very similar as well. Then, how to define these signal characteristics, and, if possible, how to combine them into one metric, are key questions. A method to accurately define the important signal characteristics is proposed in the following section.

III. Equal-Variances Method

The equal-variances method quantifies the various forcing function signal characteristics. Its purpose is to allow experimenters to better predict the effects of particular choices of the forcing function parameters on human control behavior and also to enable them to compare various forcing functions. The method will be illustrated by considering the STI 6-4 forcing function as an example. To test the method experimentally, two forcing functions with equal variance of the signal itself and its derivatives, but with different spectra, will be defined. In addition, the analysis is extended with an investigation into the effect of the phases of the sinusoidal components [φ_j in Eq. (1)] on control behavior, as these are not accounted for by the equal-variances method.

A. Forcing Function Signal Characteristics

The variance of a signal is by definition the time integral of the squared signal magnitude, i.e., a measure for the average power of the realization:

$$\sigma^2\{i(t)\} = \lim_{T\to\infty}\frac{1}{2T}\int_{-T}^{T}|i(t)|^2\,\mathrm{d}t \tag{2}$$

Substitution of a sum-of-sinusoids signal, Eq. (1), and regrouping yields

$$\begin{aligned}\sigma^2\{i(t)\} &= \lim_{T\to\infty}\frac{1}{2T}\int_{-T}^{T}\left|\sum_{j=1}^{N}A_j\sin(\omega_j t+\varphi_j)\right|^2\mathrm{d}t\\ &= \sum_{j=1}^{N}A_j^2\lim_{T\to\infty}\frac{1}{2\omega_j T}\int_{-\omega_j T+\varphi_j}^{\omega_j T+\varphi_j}|\sin(\theta)|^2\,\mathrm{d}\theta\end{aligned}$$

When the sinusoidal period fits an integer number of times within the measurement time T, the total power is equal to the power of a single full period, and the interval $[-\omega_j T+\varphi_j, \omega_j T+\varphi_j]$ equals $[-\pi,\pi]$. Since the symmetry of a squared sinusoid implies that the integral of a single full period equals two times the integral of half a period, we can obtain for the variance of a sum-of-sinusoids signal:

$$\begin{aligned}\sigma^2\{i(t)\} &= 2\sum_{j=1}^{N}A_j^2\frac{1}{2\pi}\int_0^{\pi}\sin^2(\theta)\,\mathrm{d}\theta\\ &= \sum_{j=1}^{N}A_j^2\frac{1}{\pi}\left[\frac{1}{2}\theta-\frac{1}{4}\sin(2\theta)\right]_0^{\pi}=\sum_{j=1}^{N}\frac{A_j^2}{2}\end{aligned} \tag{3}$$

The variance of the signal's first derivative can be obtained in a similar fashion and is the sum of the power content at each frequency $(A_j^2/2)$, multiplied by the square of each frequency (ω^2):

$$\sigma^2\{i'(t)\} = \lim_{T\to\infty}\frac{1}{2T}\int_{-T}^{T}|i'(t)|^2\,\mathrm{d}t = \sum_{j=1}^{N}\omega_j^2\frac{A_j^2}{2} \tag{4}$$

A general expression for the variance of the nth derivative is then given by

$$\sigma^2\left\{\frac{\mathrm{d}^n i(t)}{\mathrm{d}t^n}\right\} = \lim_{T\to\infty}\frac{1}{2T}\int_{-T}^{T}\left|\frac{\mathrm{d}^n i(t)}{\mathrm{d}t^n}\right|^2\mathrm{d}t = \sum_{j=1}^{N}\omega_j^{2n}\frac{A_j^2}{2} \tag{5}$$

For nonperiodic signals the variance can be obtained by Fourier transformation and using symmetry properties:

$$\begin{aligned}\sigma^2\{i(t)\} &= \lim_{T\to\infty}\frac{1}{2T}\int_{-T}^{T}|i(t)|^2\,\mathrm{d}t = 2\frac{1}{2T}\int_{-T/2}^{T/2}|i(t)|^2\,\mathrm{d}t\\ &= \frac{1}{\pi}\int_0^{\infty}\frac{|I(j\omega)|^2}{T}\,\mathrm{d}\omega\end{aligned} \tag{6}$$

The variance of the nth derivative of the signal can be obtained by multiplying the Fourier transform in Eq. (6) by the complex frequency vector to the power of the nth derivative:

$$\mathcal{F}\left\{\frac{\mathrm{d}^n i(t)}{\mathrm{d}t^n}\right\} = (j\omega)^n I(j\omega) \tag{7}$$

Replacing the Fourier transform with a signal's power spectral density, $\Phi_{ii}(\omega) = |I(j\omega)|^2/T$, yields a general expression for the variance of any periodic or aperiodic signal's nth-order derivative:

$$\sigma^2\left\{\frac{\mathrm{d}^n i(t)}{\mathrm{d}t^n}\right\} = \frac{1}{\pi}\int_0^{\infty}\omega^{2n}\Phi_{ii}(\omega)\,\mathrm{d}\omega \tag{8}$$

A summary of the variance expressions for forcing function signals and their derivatives is provided in Table 1.

B. Example STI 6-5 Forcing Function

Figure 3a shows the power spectral density plot of the STI 6-4 forcing function taken from [2]. Figure 3d illustrates that the low-frequency sinusoids until the bandwidth contribute to 99% of the magnitude of signal's variance; the high-frequency sinusoids add very little.

Figures 3b–3e demonstrate that, for this forcing function, about half of the magnitude of the signal's first derivative variance is due to sinusoids with frequencies around the bandwidth, further referred to as midfrequencies, whereas the other half comes from sinusoids beyond the bandwidth, called high frequencies.

In Figs. 3c–3f it is shown that the signal's second derivative variance is almost completely determined by the power of the last two high-frequency sinusoids. It is apparent that a relation exists between the variance of the nth derivative of a signal and the range in the power spectrum.

The fundamental principle of the equal-variances metric is to use this property, that is, to compare different forcing function power spectra by the values of the signal's variance and the variances of its derivatives. By considering the variances of the signal and its derivatives in combination, the power content in the different frequency regions can be weighted and signals can be better compared.

This is best exemplified by considering the variances of the first and second derivatives. It was demonstrated that the mid- and

Table 1 Definition of analytical and experimental variances of a signal and its derivatives

Variance of		Integer number of whole periods	Any periodic or aperiodic signal
Signal	$\sigma^2\{i(t)\}$	$\sum_{j=1}^{N}\frac{A_j^2}{2}$	$\frac{1}{\pi}\int_0^{\omega}\Phi_{ii}(\omega)\,\mathrm{d}\omega$
First derivative	$\sigma^2\{i'(t)\}$	$\sum_{j=1}^{N}\omega_j^2\frac{A_j^2}{2}$	$\frac{1}{\pi}\int_0^{\omega}\omega^2\Phi_{ii}(\omega)\,\mathrm{d}\omega$
Second derivative	$\sigma^2\{i''(t)\}$	$\sum_{j=1}^{N}\omega_j^4\frac{A_j^2}{2}$	$\frac{1}{\pi}\int_0^{\omega}\omega^4\Phi_{ii}(\omega)\,\mathrm{d}\omega$
nth order derivative	$\sigma^2\{\frac{\mathrm{d}^n i(t)}{\mathrm{d}t^n}\}$	$\sum_{j=1}^{N}\omega_j^{2n}\frac{A_j^2}{2}$	$\frac{1}{\pi}\int_0^{\omega}\omega^{2n}\Phi_{ii}(\omega)\,\mathrm{d}\omega$

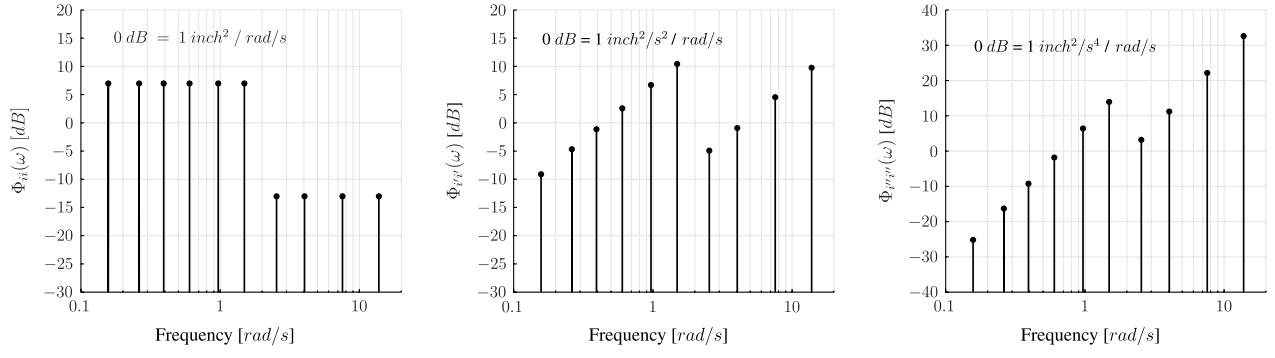

a) Forcing function power spectrum **b) First derivative power spectrum** **c) Second derivative power spectrum**

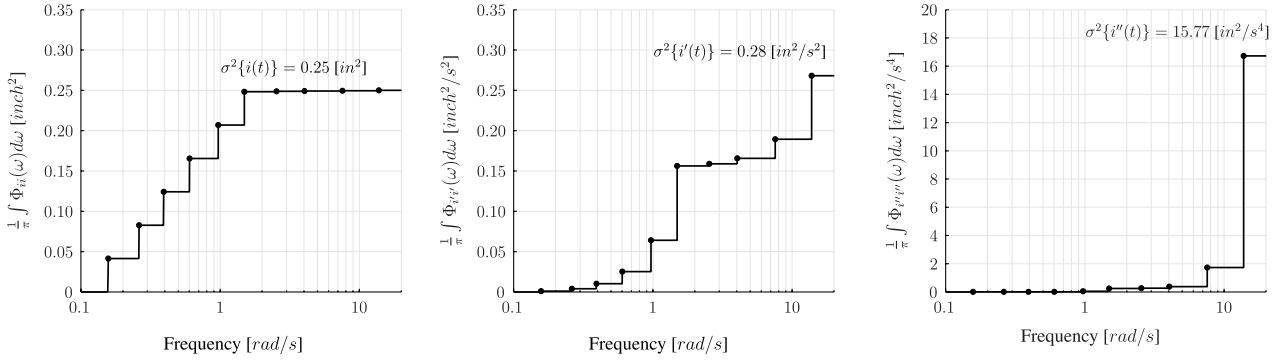

d) Integral of power spectrum **e) Integral of first derivative power spectrum** **f) Integral of second derivative power spectrum**

Fig. 3 Forcing function frequency regions confined by the frequency-weighing factors.

high-frequency power content defines the variance of the first derivative, whereas the high-frequency power content primarily determines the variance of the signal's second derivative. Hence, if one would want to limit the second derivative variance, and the variances are considered together, the influence of the first derivative variance would be reduced to midfrequencies.

Figure 4 gives an overview of the variances of three common STI forcing functions. It illustrates that the value of the signals' first derivative increases between the STI forcing functions. The variance of the second derivative is smaller for STI 7-3 than for STI 6-4. This is remarkable, as STI 7-3 turned out to be more difficult to track than STI 6-4 [2], and it might indicate that the variance of the signal's second derivative affects human control behavior to a lesser extent.

Figure 4 also contains the variance of the first and second derivatives of the STI 8-2 forcing function, which are significantly higher than those of the STI 6-4 and STI 7-3 forcing functions. This forcing function led to crossover regression with a double integrator K/s^2.

To test the validity of the equal-variances metric experimentally, two forcing functions with equal variances and variances of the higher derivatives, but with different spectra, should result in similar human control behavior. In the next subsection such forcing functions will be created.

C. Creating Forcing Functions with Equal Variances

The equal-variances metric is not limited to discrete sum-of-sinusoids spectra, so many alternatives for forcing function design can be used. To test the equal-variances metric, a set of continuous-spectra forcing functions is designed with variances equal to those of the STI 6-4, 7-3, and 8-2 spectra. Continuous-spectra forcing functions were selected because these forcing functions have a large degree of freedom to match a particular set of variances.

Although some literature is available on the design of continuous-spectra forcing functions, most attempts were not very successful. In a University of Toronto Institute for Aerospace Studies (UTIAS)

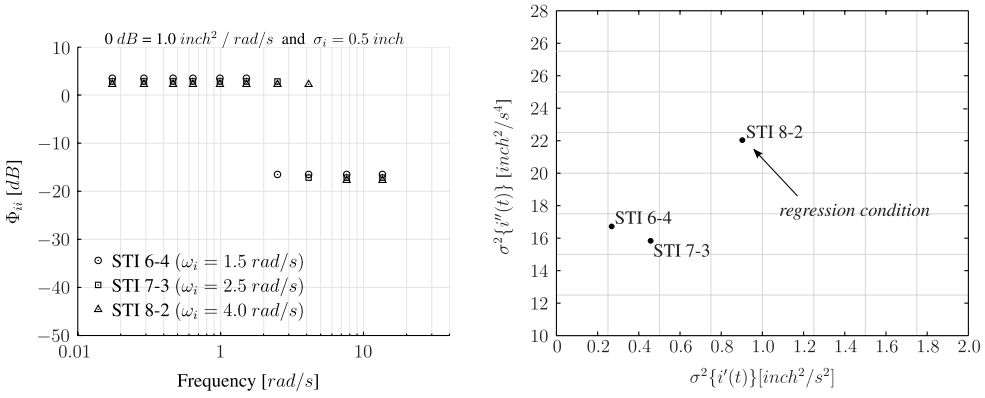

a) STI power spectral densities **b) Variances**

Fig. 4 Overview of STI forcing functions.

Table 2 Definition of shaping filter parameters

	τ_1, s	τ_2, s	τ_3, s	τ_4, s	K_{hi}, in./in.	$\omega_{N,\text{hi}}$, rad/s	K_{lo}, in./in.	$\omega_{N,\text{lo}}$, rad/s
TUD 6-4	105.4161	5.47064	2.63763	10.1554	0.057498	14.1422936	2.22867	1.347792
TUD 7-3	31.16206	6.89872	1.21247	2.48055	0.028064	14.0367261	0.90166	2.063390
TUD 8-2	1.358535	2.30793	0.15626	79.12585	0.15819	13.8082431	3.55535	3.750531

investigation, for example, it was found to be rather difficult to design a continuous-spectrum forcing function with a 20 dB drop in power at high frequencies [8]. The UTIAS forcing function had been designed to contain a bandwidth equivalent to the STI sum-of-sinusoids step-shaped forcing functions according to [1,2,8]:

$$\omega_{ie} = \left(\int_0^\infty \Phi_{ii}(j\omega)\,\mathrm{d}\omega\right)^2 \Big/ \int_0^\infty (\Phi_{ii}(j\omega))^2\,\mathrm{d}\omega \tag{9}$$

Although the UTIAS spectra had the same equivalent bandwidth as the STI spectra, the UTIAS forcing functions resulted in crossover regression [8]. It will be shown below that the variances for the UTIAS forcing functions are 10 to several hundred times larger than those of the STI spectra. Designing continuous-spectrum forcing functions while keeping the variance and the variance of the derivatives equal could resolve this problem.

A set of continuous-spectrum forcing functions was developed in three stages. First, the transfer function of a shaping filter was chosen with enough degrees of freedom to allow sufficient manipulation of the variance of the first five derivatives (including the zero-order derivative, the signal itself). In the second stage, the filter parameters were determined using an optimization algorithm that minimizes the differences between the variances of the resulting shaping filter and those of the reference forcing function. In the third stage the time-domain realizations were computed, by driving the shaping filter transfer functions with Gaussian white noise. The three stages are discussed below.

1. *Stage 1: Continuous-Spectrum Shaping Filter*

The spectral shaping transfer functions were divided in a high-power, low-frequency component $B(j\omega)$ and an attenuated high-frequency component $C(j\omega)$, very similar to the discrete STI spectral shapes. The two components together make up the shaping filter transfer function $F(j\omega)$:

$$F(j\omega) = \underbrace{B(j\omega)}_{\text{low-frequency component}} + \underbrace{C(j\omega)}_{\text{high-frequency component}} \tag{10}$$

where

$$B(j\omega) = K_{\text{lo}}\left(1 + \frac{1}{\tau_1 j\omega + 1}\right)\text{butterworth}(O_{\text{lo}}, \omega_{N,\text{lo}}) \tag{11}$$

and

$$C(j\omega) = K_{\text{hi}}\left(1 + \frac{1}{\tau_2 j\omega + 1} + \frac{1}{\tau_3 j\omega + 1} + \frac{1}{\tau_4 j\omega + 1}\right)\text{butterworth}(O_{\text{hi}}, \omega_{N,\text{hi}}) \tag{12}$$

The orders of the low-frequency and high-frequency butterworth filter were, respectively, 8th and 9th order. The eight remaining parameters of Eqs. (11) and (12) were computed by performing an optimization that minimized a mean-squared criterion function Δ:

$$\Delta = \sum_{j=0}^{4}\left(\frac{|\sigma^2\{\frac{\mathrm{d}^n}{\mathrm{d}t^n} i_{\text{shaping filter}}(t)\} - \sigma^2\{\frac{\mathrm{d}^n}{\mathrm{d}t^n} i_{\text{reference}}(t)\}|}{\sigma^2\{\frac{\mathrm{d}^n}{\mathrm{d}t^n} i_{\text{reference}}(t)\}}\right)^2 \tag{13}$$

2. *Stage 2: Parameter Search by Hybrid Optimization*

Equation (13) governs a parameter space with many local minima. Simple gradient-search algorithms converged to local minima. Better results were obtained by a combination of genetic and gradient-search algorithms. Multiple optimizations were performed to ensure a global minimum. The resulting parameters are summarized in Table 2. The resulting shapes will be referred to as Delft University of Technology (TUD) 6-4, 7-3, and 8-2.

Figures 5 and 6 illustrate that the TUD spectra have less power at high frequencies than the UTIAS spectra (and the STI spectra, not shown in Figs. 5 and 6). Whether these continuous TUD spectra still provide enough power to yield sufficient signal-to-noise ratios at higher frequencies will be discussed in Sec. V.

The STI, UTIAS, and TUD frequency-weighing factors are listed in Table 3. Comparison of the UTIAS and STI variances indeed reveals very large differences in the higher frequency-weighing factors, a direct consequence of the 20 dB power attenuation in the UTIAS spectra. The TUD spectra frequency-weighing factors are very similar to those of the original STI spectra.

3. *Stage 3: Generating Time-Domain Realizations*

The time histories in Fig. 7 were generated using Gaussian white noise. Whereas the TUD signals resemble the STI signals, the UTIAS time-domain realizations are rather different. The STI and TUD signals have been used in the experiment in Sec. IV.

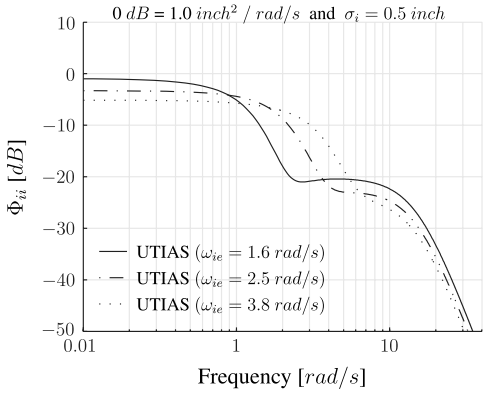

Fig. 5 UTIAS power spectral densities.

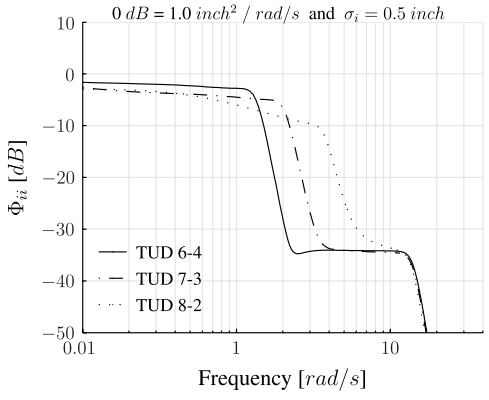

Fig. 6 TUD power spectral densities.

Table 3 Variances of the STI, UTIAS, and TUD spectra forcing functions

Forcing function	Bandwidth	$\sigma^2\{i(t)\}$, in.^{2}	$\sigma^2\{\frac{di(t)}{dt}\}$, in.^{2}/s^2	$\sigma^2\{\frac{d^2i(t)}{dt^2}\}$, in.^{2}/s^4	$\sigma^2\{\frac{d^3i(t)}{dt^3}\}$, in.^{2}/s^8	$\sigma^2\{\frac{d^4i(t)}{dt^4}\}$, in.^{2}/s^{16}	Δ from reference, %
STI 6-4	($\omega_i = 1.5$ rad/s	0.25	0.27559	15.7721	2651.4	476,549	——
TUD 6-4	($\omega_{ie} = 1.4$ rad/s	0.25	0.27559	15.7721	2537.6	476,552	4.33
UTIAS	($\omega_{ie} = 1.6$ rad/s	0.25	2.5365	550.836	377,494	2.3×10^9	5103
STI 7-3	($\omega_i = 2.5$ rad/s	0.25	0.45709	14.9297	2286.7	409,493	——
TUD 7-3	($\omega_{ie} = 2.5$ rad/s)	0.25	0.45709	14.9297	2226.7	410,373	2.85
UTIAS	($\omega_{ie} = 2.5$ rad/s)	0.25	1.7533	323.106	220,642	1.3×10^9	3440
STI 8-2	($\omega_i = 4.0$ rad/s)	0.25	0.9272	22.07	2157.7	361,559	——
TUD 8-2	($\omega_{ie} = 2.9$ rad/s)	0.25	0.9294	21.82	2194.1	361,438	3.08
UTIAS	($\omega_{ie} = 3.8$ rad/s)	0.25	1.89	227.56	147,177	8.9×10^8	2542

D. Effect of Phases

Designing a forcing function based on the variance of the derivatives incorporates the amplitudes A_j and the frequencies ω_j in Eq. (1). The remainder of this section will discuss the effect of the phases φ_j by examining the amplitude distribution of the time-domain realizations.

In nonlinear system identification, the amplitude distribution of a time-domain realization affects the parameters of the fitted model [21,22]. The amplitude distribution determines which amplitudes of the nonlinear system are emphasized in the excitation process. This is illustrated in Fig. 8, which shows the fit of a line to a nonlinear arc-tangent function, driven each time by an input signal that has a different amplitude distribution. A Gaussian distribution excites the arc tangent in such a way that the linear polynomial fit emphasizes the arc tangent around its origin; when exciting with a signal that has a sinusoidal amplitude distribution, the fit of large amplitudes of the arc tangent is emphasized.

Table 4 gives an overview of the mean-squared errors-of-fit between the fitted line and the nonlinear arc tangent for inputs with different amplitude distributions. Apparently, the discrepancy between the describing function and the nonlinear model is minimal if both are excited by a signal with the same amplitude distribution. Overall, the Gaussian excitation yields the lowest absolute mean-squared error. This does, however, not imply that Gaussian excitation yields the best fit of a linear polynomial to a nonlinear model. The amplitude distribution resulting in the lowest mean-squared error-of-fit depends on the nature of the nonlinear model.

For the identification of human control behavior it is important that the control task resembles a real-life control situation [2]. The central limit theorem states that in the limit case all real-life perturbations will tend to be Gaussian and so will be the real-life control behavior. Therefore, signals with Gaussian amplitude distributions are preferred.

A forcing function signal can be broken down into sinusoidal components with an associated phase. Depending on the value of the phase of each of the sinusoidal components at certain periods in time the sinusoidal components will amplify or attenuate each other. These periods vary as the power spectrum or phases are changed. Hence, for different spectra or phases these periods occur at different times and with different intensities. To the best of our knowledge, no insights nor literature are available in which the effect of the phases of each of the sine components of the forcing function on the human

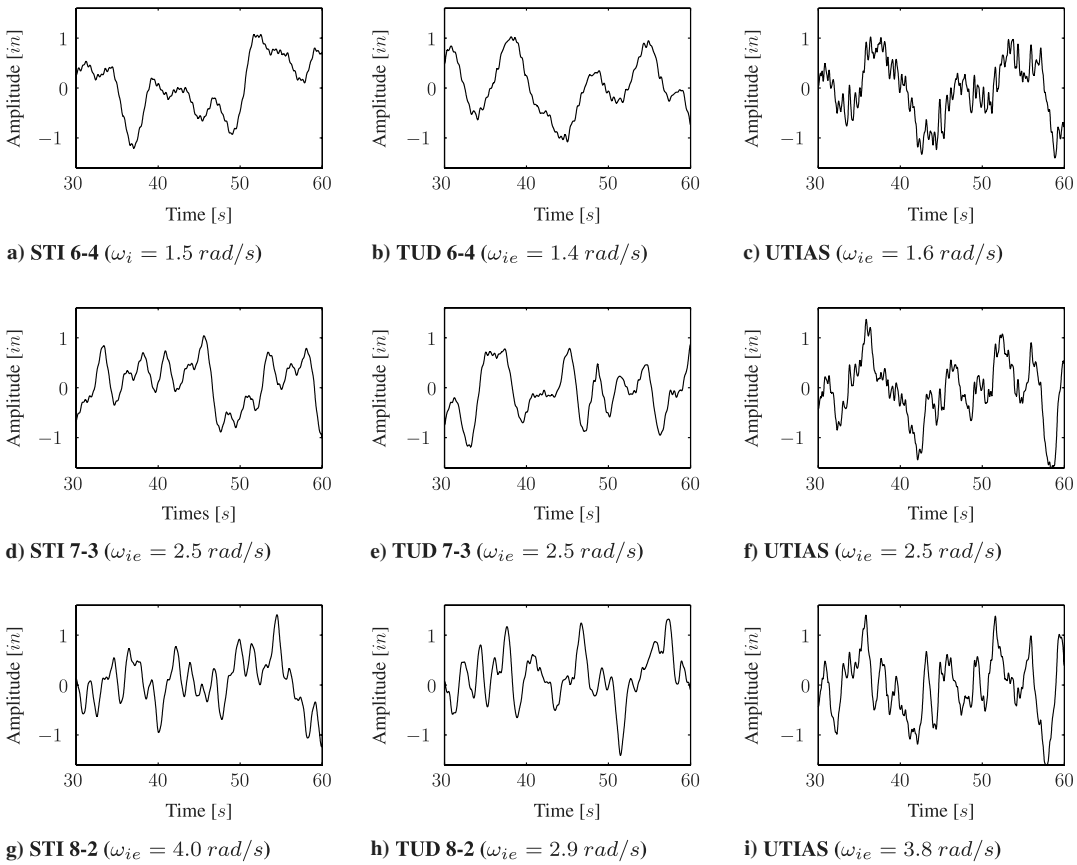

a) STI 6-4 ($\omega_i = 1.5\ rad/s$) **b) TUD 6-4** ($\omega_{ie} = 1.4\ rad/s$) **c) UTIAS** ($\omega_{ie} = 1.6\ rad/s$)

d) STI 7-3 ($\omega_{ie} = 2.5\ rad/s$) **e) TUD 7-3** ($\omega_{ie} = 2.5\ rad/s$) **f) UTIAS** ($\omega_{ie} = 2.5\ rad/s$)

g) STI 8-2 ($\omega_{ie} = 4.0\ rad/s$) **h) TUD 8-2** ($\omega_{ie} = 2.9\ rad/s$) **i) UTIAS** ($\omega_{ie} = 3.8\ rad/s$)

Fig. 7 Comparison of time history characteristics of the STI, TUD, and UTIAS spectra.

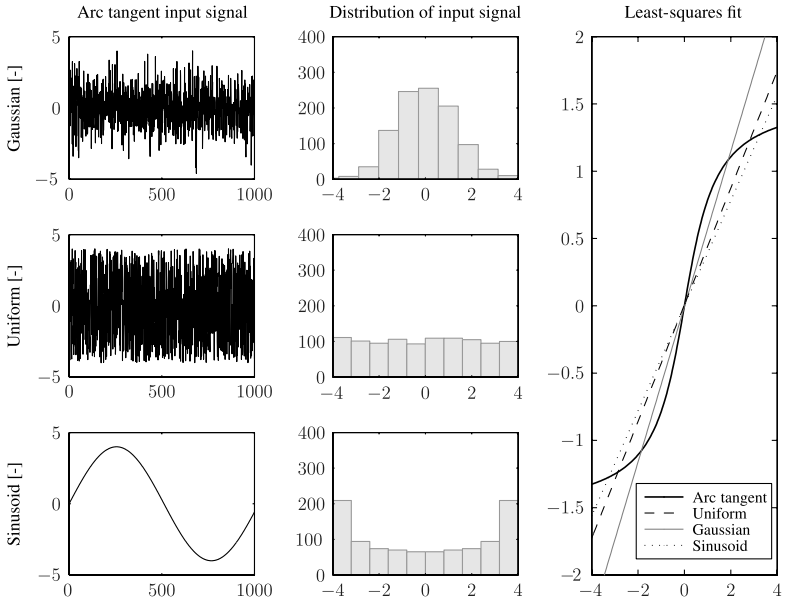

Fig. 8 Linear fits to a nonlinear arc-tangent function driven by different amplitude distributions [21].

control behavior is considered. For this reason, the effects of the phases will be included in the experimental analysis, discussed in the next section.

IV. Experiment

The experiment was designed to test the following main hypotheses:

1) Operator control behavior will be affected by the phase set definitions. To check the validity of this hypothesis, the forcing function definitions with different phase sets will be used.

2) Operator control behavior with different forcing functions will only be the same if all the variances of the forcing functions and its derivatives are the same.

A more detailed description of these hypotheses is presented in Sec. IV.H. Our objective in designing this experiment was to replicate some of the conditions of the original 1965 experiment carried out by McRuer et al. [2] at Systems Technology, Inc. This way, the original experiment can provide us with validated reference values for human performance and control behavior.

A. Original STI Experiment

The 1965 STI experiment featured a visual compensatory tracking task and involved proportional-, rate-, and acceleration-controlled element dynamics. The manipulator was a spring-restrained lateral sidestick with extreme positions of $\pm 15°$. The moment arm was 4 in. (or 10.16 cm). Deflection sensitivity for acceleration control was defined as $0.167K_c$ in./s^2 on the display per degree stick deflection, with K_c the controlled element gain. The stick dynamics were defined as a spring-force equivalent to 2.21 oz/ deg at the top of the 4 in. moment arm. The inertia and damping were negligible. Movements of the stick in one direction produced system outputs in the same direction. Eye-to-display distance was kept constant at 29 in.

Table 4 Mean-squared error-of-fit associated to different amplitude distributions

	First-order linear polynomial driven by		
Nonlinear arc tangent driven by	Uniform	Gaussian	Sinusoid
Uniform	0.242	0.261	0.278
Gaussian	0.433	0.170	0.630
Sinusoid	0.266	0.306	0.242

Subjects in the STI experiment were two highly experienced civilian engineering test pilots, six naval test pilots, and one light-aircraft-qualified civilian pilot with extensive training. Not all pilots were involved with all type of controlled elements. Only five subjects participated in the acceleration-control measurements. At least 10 and often 20 training runs of 2 min duration each were performed until a stable level of performance was reached, measured in normalized mean-squared error $\bar{e}^2/\sigma_i^2$. Then, two 4-min runs were recorded. In the recorded runs, a run-in time of 10 to 15 s preceded the 240 s measurement time T.

The three basic types of controlled element dynamics were factorially combined with the three forcing functions introduced earlier, i.e., STI 6-4, 7-3, and 8-2. The forcing function magnitudes were standardized to a standard deviation of 0.5 in.; this was experimentally determined to be both realistic and trackable for most of the conditions. The magnitudes of the sinusoids at frequencies beyond the bandwidth were set to a tenth of the low-frequency sinusoids; i.e., power was attenuated 20 dB. The time histories of the forcing functions were tested for a Gaussian distribution at the 95% confidence interval.

Dependent measures were the mean-squared tracking error, operator crossover frequency and phase margin, linear correlation coefficients, and control behavior model parameters.

B. Replication: Current Experiment Setup

To replicate the 1965 STI experiment a compensatory tracking task with central foveal display was set up in our laboratory as depicted in Fig. 9a. Only pure acceleration-control, $Y_c(j\omega) = K_c/(j\omega)^2$, was used in the present experiment. The controlled dynamics gain K_c was fixed at 5 in./in.

Although the original experiment also featured gain and integrator dynamics, these were not included in the present experiment. Because of time constraints and the large number of forcing functions to be tested it was decided to limit the number of controlled elements to one. The gain element was the least suited for the experiment since it provides state information through the control inceptor. As such it is not a pure compensatory situation and the forcing function might be better predictable by the subjects. The double integrator appeared the most interesting for its demonstrated potential to result in crossover regression at high forcing function bandwidths and was therefore chosen over the rate-controlled element Nevertheless, it is recommended to perform an additional study of the effects of the forcing function design with a rate system.

The control manipulator was an electrohydraulic sidestick with 1 degree of freedom (lateral). The moment arm was 9 cm. To replicate

a) Experimental setup showing display and side-stick

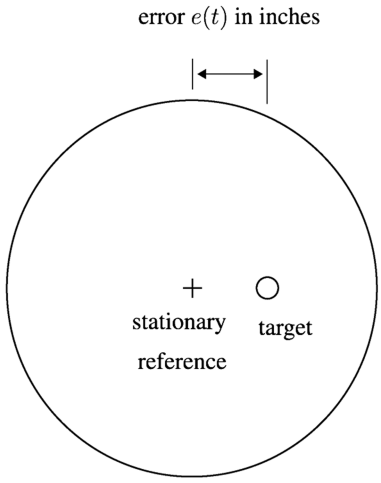

b) Display layout equivalent to the STI display [2]

Fig. 9 Experiment setup.

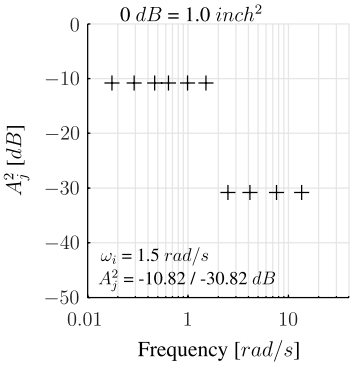

Fig. 10 Power spectral density plot of the modified STI 6-4 spectrum (Ax_{6-4}), standardized to $\sigma_i = 0.5$ in.

the spring-restrained sidestick dynamics in the STI experiment, the torsional stiffness was set at 3.5766 Nm/rad, while torsional damping and mass were kept as low as possible at 0.08 Nms/rad and 0.01 kg m^2, respectively.

Subjects were seated in an adjustable chair in a low-noise, darkened room. They were instructed to keep the eye-to-display distance constant at approximately 29 in. (74 cm). Subjects were presented a display, showing a stationary reference (cross), fixed at the center of the screen and a target (circle) that moved in lateral direction (see Fig. 9b). The stationary reference and target were displayed in green on a black background. The frame of reference was inside out, implying that the reference (cross) had to be steered toward the target (circle). The display size and layout were exactly the same as the STI display. The value of the display gain was selected such that the instantaneous tracking error e could be directly read off the display in inches.

The experiment consisted of two phases:

1) The first phase was a training phase. Here, subjects got familiar with the experiment. As will be discussed below, the experimental conditions were divided in three categories: easy, baseline, and difficult. For each category, it was determined what type of control strategy resulted in the lowest normalized tracking error $\bar{e}^2/\sigma_i^2$. Training was continued until reasonable levels of stationary tracking performance were obtained; an average of 120 training runs were performed per subject.

2) The second phase was the measurement phase. The data of five successive runs for each condition were recorded for postexperiment evaluation.

The experiment was designed in such a way that per subject all conditions were randomly distributed. To minimize changes in control strategy during measurement runs, the category of each condition was made clear before each run so that the subject could associate the nature of the run with the selected control strategy in the training phase.

C. Independent Variables

The independent variable in the experiment is the forcing function. A total number of 10 distinct forcing function conditions

Table 5 Definition of forcing function periods and frequencies

Conditions Ax_{6-4}, B_{7-3}, and F_{8-2}				Condition C_{8-3}			Condition D_{6-5}		
Modified STI forcing functions				Additional sinusoids at bandwidth			Additional sinusoids at high frequencies		
i	Period	ω_i, rad/s	ω_i orig STI, rad/s	i	Period	ω_i, rad/s	i	Period	ω_i, rad/s
1	3	0.175	0.157	1	5	0.291	1	5	0.291
2	5	0.291	0.262	2	8	0.465	2	8	0.465
3	8	0.465	0.393	3	11	0.640	3	11	0.640
4	11	0.640	0.602	4	17	0.989	4	17	0.989
5	17	0.989	0.969	5	26	1.51	5	26	1.51
6	26	1.51	1.49	6	**38**	2.21	6	43	2.50
7	43	2.50	2.54	7	**41**	2.39	7	71	4.13
8	71	4.13	4.03	8	43	2.50	8	131	7.62
9	131	7.62	7.57	9	71	4.13	9	**181**	10.53
10	233	13.56	13.8	10	131	7.62	10	233	13.56
				11	233	13.56	11	**327**	19.02

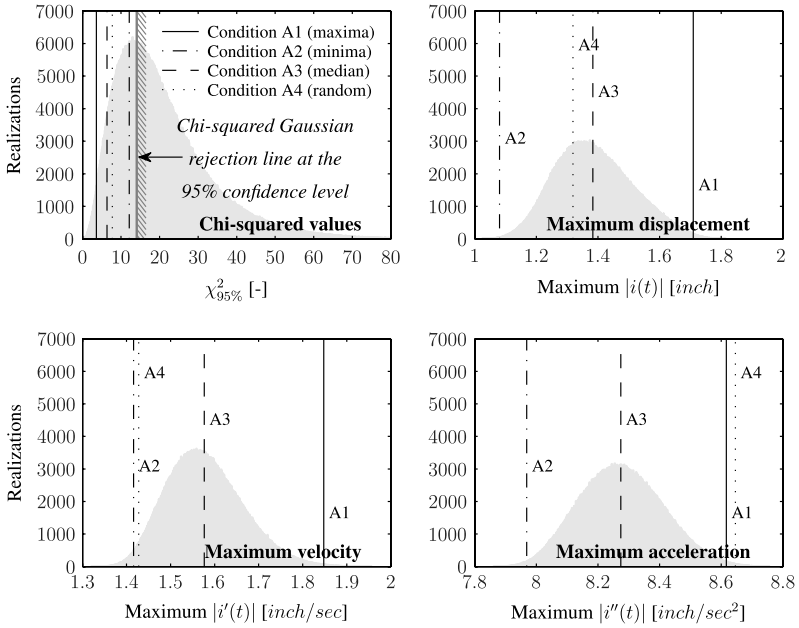

Fig. 11 Chi-squared and maximum displacement, velocity, and acceleration distributions.

were tested, all based on the original STI 6-4, 7-3, and 8-2 forcing functions.

Instead of the original STI forcing functions, slightly modified versions were used. To prevent fatigue and obtain stationary control behavior, while at the same time maintaining enough frequencies without power around the low-frequency sinusoids, the measurement time of all experiments was limited to 108 s, instead of 240 s in the STI experiment. As a result, the base frequency $2\pi/T$ changed, and the frequencies used in the forcing functions only approximated the original STI frequencies.

An implication of the shorter run duration was a decrement of the number of periods of the sines in the forcing function. For instance, the sine with the lowest frequency in the original McRuer et al. [2] forcing function ($\omega_i = 0.157$ rad/s) had six periods in the original 240 s run, whereas its equivalent ($\omega_i = 0.175$ rad/s) in the modified forcing function only had three periods in the 108 s run. In the original experiment the pilot frequency response was estimated at the individual frequencies of the forcing function sine components using Foerier coefficients. The reduced number of periods results in a lower power-to-noise ratio at the frequencies of the forcing function sines, and consequently leads to higher biases and larger variance at these frequencies, reducing the accuracy of the estimated frequency response. This is especially a problem at the lowest frequencies. Newer identification methods, such as the autoregressive-with-exogenous-inputs-model (ARX) and maximum-likelihood-estimation (MLE) methods, are capable of identifying a frequency response over the full frequency domain due to a model-based approach. Therefore, they are less sensitive to low power-to-noise ratios at low frequencies.

We have performed trial experiments with the original and the reduced run durations. The identification accuracy, in terms of variance accounted for, appeared adequate to allow the shorter run durations.

The 10 forcing function conditions will be introduced in the remainder of this section.

1. Effect of Phases

The first four conditions, $A1_{6-4}$ until $A4_{6-4}$, were all based on the slightly modified STI 6-4 spectrum, shown in Fig. 10. The frequencies are listed in Table 5.

Four distinct phase sets were selected using Fig. 11, which shows the results of the simulation of 100,000 forcing functions with random phases. Displayed are the χ^2 value, the absolute maximum displacement, velocity, and acceleration. Only forcing functions with an χ^2 value with the 95% confidence interval could be used to assure a Gaussian distribution.

Based on the assumption that the most volatile effects due to the phases would occur somewhere around a maximum displacement, velocity, or acceleration in the signal realization, condition $A1_{6-4}$ was defined. The opposite, i.e., having minimum displacement, velocity, and acceleration was defined as condition $A2_{6-4}$. Condition $A3_{6-4}$ was chosen as close to the median of the displacement, velocity, and acceleration maxima distributions. To account for the possibility that the selected phase sets were selected on invalid grounds, the phases of condition $A4_{6-4}$ were chosen at random. The resulting phase sets are listed in Table 6.

2. Effects of Bandwidth and Variances

The next four forcing functions, B_{7-3}, C_{8-3}, D_{6-5} (see Fig. 12), and E_{7-3}, all had a bandwidth of 2.5 rad/s and equal signal power. The reference, condition B_{7-3}, was the STI 7-3 spectrum forcing function, with first derivative variance equal to 0.457 $\text{in.}^2/\text{s}^2$.

Condition E_{7-3} was the continuous-spectrum forcing function that had the same variances of the first five derivatives as B_{7-3} (i.e., TUD 7-3 in Table 2). It was included in the experiment to test the equal-variances metric at this particular bandwidth. That is, since B_{7-3} and E_{7-3} have approximately equal variances, human control behavior as a result of these two forcing functions is hypothesized to be the same.

Table 6 Phases of forcing function conditions $A1_{6-4}$–$A4_{6-4}$

	Phase φ_j of sinusoid j, deg									
Condition	1	2	3	4	5	6	7	8	9	10
$A1_{6-4}$ (maxima)	0.3664	0.9182	0.1611	6.2431	5.2318	3.7561	1.2981	1.8351	3.8561	4.8764
$A2_{6-4}$ (minima)	6.0427	4.4901	3.3944	4.5053	2.2796	3.9873	3.9956	0.1480	6.2613	3.0741
$A3_{6-4}$ (median)	1.2691	4.9538	0.1545	1.0368	2.4102	0.4583	5.9714	5.8774	4.0589	1.8445
$A4_{6-4}$ (random)	1.6444	4.5985	3.8301	1.7720	5.4522	1.0435	2.3720	5.4235	2.3301	5.0249

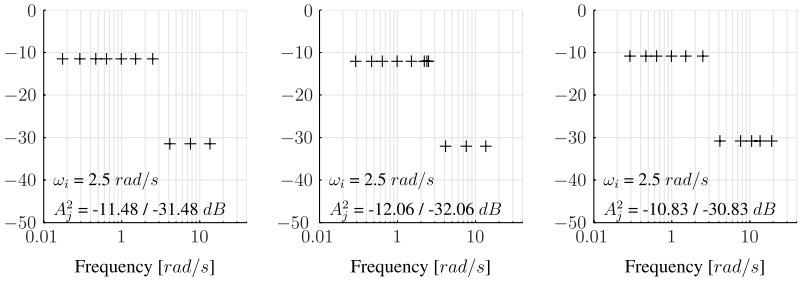

a) Condition B_{7-3} **b) Condition C_{8-3}** **c) Condition D_{6-5}**

Fig. 12 Power spectral density plot of the modified STI 7-3 spectra, standardized to $\sigma_i = 0.5$ in.

Condition C_{8-3} was equal to B_{7-3}, except that two additional sinusoidal components were inserted just below the bandwidth frequency, i.e., at 2.21 and 2.39 rad/s. The variance of this signal's first derivative was different: 0.728 in.^{2}/s^2. Condition D_{6-5} was constructed to have a similar first derivative variance as C_{8-3} (0.725 in.^{2}/s^2), but now included two high-frequency sinusoids at 10.5 and 19 rad/s. To maintain sufficient power at the sinusoids' frequencies, for both the conditions C_{8-3} and D_{6-5} the lowest-frequency sinusoid of the reference condition B_{7-3} was left out. The additional sinusoidal components are set in boldface in Table 5.

The rationale of including forcing functions C_{8-3} and D_{6-5} in the experiment was as follows. Consider Fig. 13, which shows the input-to-error transfer function e/i with human control behavior as predicted by McRuer et al's [2] crossover model $[Y_c(\omega)Y_p(\omega) = (\omega_c/j\omega)e^{-j\omega\tau_e}]$, with a crossover frequency $\omega_c = 2$ rad/s and equivalent time delay $\tau_e = 0.45$ s. The figure illustrates that, whereas the operator is successful in reducing the effects of the low-frequency sinusoidal components, the higher frequency components are not affected at all. It also shows that the frequency components near and just beyond the operator's crossover frequency are actually amplified by the operator control actions.

We hypothesized that placing additional sinusoidal components just below the forcing function bandwidth (condition C_{8-3}) would force operators to change their control strategy in such a way that the resulting e/i characteristic would reduce the effects of the sinusoidal components around the crossover region.

When placing the additional sinusoidal components above the operator crossover region (condition D_{6-5}) it is unclear what would happen. On the one hand, the e/i characteristic indicates that these frequency components cannot be reduced, and one possible hypothesis could be that, since the operator cannot do much about these signals, he or she will not adapt. But, on the other hand, when these high-frequency sinusoidal components would always appear in the error, this could negatively influence the operator's ability to generate lead (i.e., differentiate the signal), which is mandatory for the double-integrator-dynamics-controlled element in this experiment.

The last two forcing functions, F_{8-2} (see Fig. 14) and G_{8-2}, both had a bandwidth of 4.0 rad/s and equal power. The reference, condition F_{8-2}, was the STI 8-2 spectrum forcing function. Condition G_{8-2} was the equivalent frequency-weighing factors continuous-spectrum forcing function (TUD 8-2 of Table 2). Since the variance of the first five derivatives (including the signal itself) were approximately equal, it was hypothesized that the resulting operator control behavior would be the same. In McRuer et al.'s [2] 1965 experiment, the F_{8-2} condition resulted in crossover regression, and it is therefore of interest here whether we will find the same regression effects for the continuous-spectrum forcing function G_{8-2}.

The expected difficulty of the forcing functions was: easy (Ax_{6-4}), baseline (B_{7-3}, C_{8-3}, D_{6-5}, and E_{7-3}), and difficult (F_{8-2} and G_{8-2}). In fact, it is hypothesized that in the latter two conditions crossover regression will occur [2].

All forcing functions were tested for a Gaussian amplitude distribution by the chi-squared criterion. The criterion tests the hypothesis, that the forcing function realization is from a Gaussian distribution. Note that the chi-squared criterion of a discrete signal is biased by the sampling rate f_s and observation time T. It is assumed, however, that a more-than-one-minute measurement time is sufficiently long to prevent the Gaussian hypothesis from being rejected by pure chance. The effect of the sampling frequency was compensated by reducing the number of forcing function samples to the highest sinusoids period, i.e., 233 for the STI spectra (Table 5). The chi-squared criterion was evaluated with 10 bins.

D. Subjects and Procedure

Five subjects, all males, participated. They were instructed to keep the reference symbol as accurately as possible superimposed on the target symbol, i.e., minimize error (see Fig. 9b). An overview of the subjects' characteristics is given in Table 7. Subjects were selected on the basis of having excellent tracking skills in order to replicate the performance results of the STI experiment subjects as close as possible. Their motivation was enhanced by actively holding track of

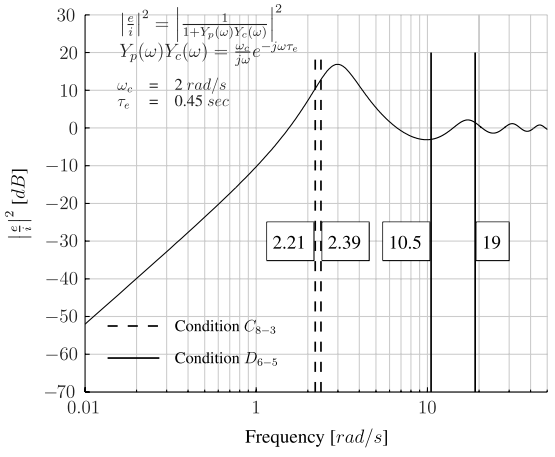

Fig. 13 Definition of additional sinusoids and closed-loop input-to-error relation.

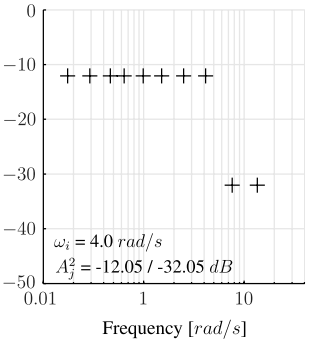

Fig. 14 Power spectral density plot of the modified STI 8-2 spectrum (F_{8-2}), standardized to $\sigma_i = 0.5$ in.

Table 7 Nature of subjects and tracking experience

Subject no.	Age	Handedness	Glasses/ lenses	Tracking experience, h
1	27	Right	——	Extensive (∼30)
2	19	Right	——	Modest (∼10)
3	26	Left	——	Extensive (∼50)
4	40	Right	——	Very extensive (>200)
5	22	Right	Lenses	Modest (∼10)

personal record on mean-squared error values, and by stimulating competition among the subjects.

For each 108 s measurement run, 10 s run-in time and 2 s run-out time were added. Thus, every run lasted 2 min. Of the 10 s run-in time, the first 5 s were used to fade-in the forcing function.

E. Limitations in the Replication of the 1965 STI Experiment

There were some aspects that could not be exactly replicated in our experiment. First, the STI experiment featured an analogous cathode ray tube display [18], where our experiment featured a low-latency, high-resolution liquid crystal display.

Second, no mention is made in the 1965 STI report about how subjects held the stick. Although a later 1974 STI report [19] briefly describes an experiment setup that is very similar to the 1965 STI experiment, and reports that the stick was "grasped between thumb and forefinger," it could be possible that this grasp was different. In our experiment, the stick was grasped with the full hand, similar to aircraft control behavior.

In addition, the original specifications of the unique inceptor in the McRuer et al. [2] experiment could not be replicated entirely by our electrohydraulic sidestick. Torsional damping and mass were kept as low as possible but are assumed to be higher than those of the original inceptor. In precision control tasks the human controller can apply muscle cocontraction to increase his neuromuscular stiffness in order to stabilize his joints [23]. It is speculated that the increased mass and damping of our inceptor might have caused a similar stabilizing effect, and better performance, compared with the very light tracker used in the original experiment.

Finally, the STI subjects were skilled subjects with extensive real-world piloting experience. Although our subjects were carefully selected highly skilled subjects, none of them had extensive real-world piloting experience.

F. Operator Control Behavior Modeling and Identification

1. Human Operator Models

Human operator control behavior was modeled by adopting one of the most accurate linear model structures, McRuer et al.'s [2] precision model[¶]:

$$Y_p(j\omega) = K_p \frac{(\tau_L j\omega + 1)}{(\tau_l j\omega + 1)} e^{-j\omega\tau_d} \frac{\omega_{\text{nm}}^2}{(j\omega)^2 + 2\xi_{\text{nm}}\omega_{\text{nm}} j\omega + \omega_{\text{nm}}^2} \quad (14)$$

This model takes into account the effects of the human equalization (first two terms), a pure time delay (third term), and the limb-manipulator neuromuscular dynamics (fourth term). The precision model can approximate the fairly linear pilot control characteristics in the crossover region rather well, including the effects of limb-manipulator neuromuscular dynamics [2], using just five parameters: K_p, τ_L, τ_d, ω_{nm}, and ζ_{nm}.[**]

The linear control behavior model parameters were obtained from the measured data using both nonparametric as well as parametric identification techniques.

[¶]Note that we omitted the very low-frequency neuromuscular system lag [2].

[**]Because double-integrator dynamics are considered, the lag-time constant τ_l can be neglected.

2. Nonparametric Identification

Two methods were used to obtain nonparametric describing functions from the measured data. The first method was the two-step Fourier coefficients (FC) method, which fits the human model to the sinusoids' frequencies in the frequency domain [2,3,24]. At these frequencies the human concentrates control power so that high signal-to-noise ratios are present. Second, the ARX method was used [16,17]. Contrary to the FC method, ARX fits linear polynomials to time-domain signals by solving an analytical least-squares criterion.

3. Parametric Identification

The time-domain MLE method was used to estimate the precision model parameters [5,17]. The main advantages of this method are that, first, the variance of the parameter estimate achieves the Cramér–Rao lower bound (i.e., is asymptotically efficient), and, second, that the estimate becomes unbiased (i.e., asymptotically unbiased), both when the observation time approaches infinity [17].

The principle is to find the joint-probability density function for predicted error ε (i.e., the difference between the measured and modeled control signal) that makes the parameter estimate $\hat{\theta}$ most likely, through maximizing the likelihood function:

$$L(\theta) = f(\varepsilon_1, \varepsilon_1, \ldots, \varepsilon_N; \theta) \quad (15)$$

The parameter vector $\hat{\theta}^{\text{mle}}$ that maximizes the likelihood function is defined by

$$\hat{\theta}^{\text{mle}} = \arg\max_{\theta} \ell_n L(\theta) = \arg\min_{\theta} \frac{1}{2\sigma_\varepsilon^2} \sum_{i=1}^{N} \varepsilon_i^2 \quad (16)$$

The convex Gauss–Newton optimization method was used to find the maximum log likelihood. This method does not guarantee finding the global minimum, thus multiple initial conditions were tried. Then, when all the initial conditions converged to the same minimum, it was assumed that a global minimum was found.

A measure for the amount of information conveyed about the parameter estimate $\hat{\theta}^{\text{mle}}$ in the data set was obtained by calculating the Fisher information matrix. The inverse of the Fisher matrix equals the Cramér–Rao lower bound, i.e., the minimum achievable variance of estimate $\hat{\theta}^{\text{mle}}$. Finally, the variance-accounted-for is computed as a measure for the linearity and model validity [16].

A typical open-loop estimate is shown in Fig. 15 ($A1_{6-4}$ condition, subject 1).

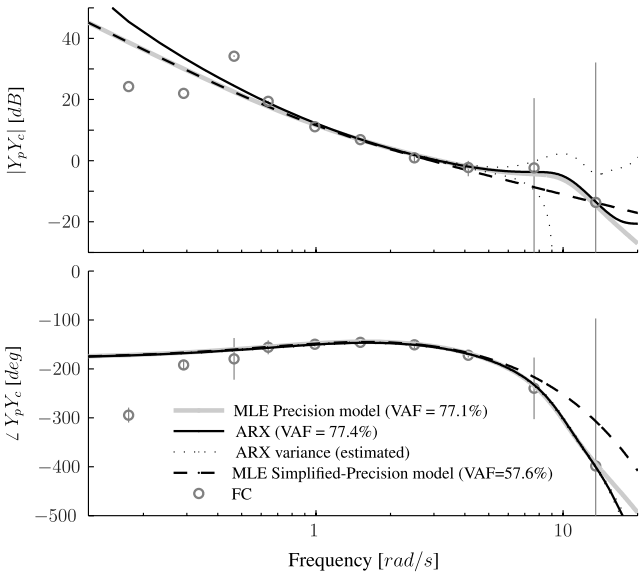

Fig. 15 Open-loop estimates of human operator and controlled dynamics.

Table 8 Relation between the independent variables and the hypotheses

		Independent variables									
Hypothesis	Step	$A1_{6-4}$	$A2_{6-4}$	$A3_{6-4}$	$A4_{6-4}$	B_{7-3}	C_{8-3}	D_{6-5}	E_{7-3}	F_{8-2}	G_{8-2}
1	——	*X*	*X*	*X*	*X*	——	——	——	——	——	——
2a	1	——	——	——	——	*X*	*X*	*X*	——	——	——
2b	2	——	——	——	——	——	*X*	*X*	——	——	——
2c	3	——	——	——	——	*Y*[a]	——	——	*Y*	*Z*[b]	*Z*

[a]Effect within group. [b]Effect within group.

G. Dependent Measures

The dependent measures included several metrics for human performance and control behavior. Time-domain performance was obtained by calculating the mean-squared values of the error and control signals. Frequency-domain control behavior metrics were the operator crossover frequency and phase margin and the five precision model parameters.

H. Hypotheses

The hypotheses follow in a straightforward way from the definitions of the forcing functions, the only independent variables in this experiment, and are summarized in Table 8.

1) The first main hypothesis in this paper is that operator control behavior will be affected by the phase set definitions. To check the validity of this hypothesis, the forcing function definitions with different phase sets will be used, i.e., $A1_{6-4}$ until $A4_{6-4}$.

2) The second main hypothesis is that operator control behavior with different forcing functions will only be the same if all the variances of the signal and its derivatives are the same. The forcing functions have been defined in such a way that we can check the validity of this hypothesis in three consecutive steps:

a) In the first step, using forcing functions B_{7-3}, C_{8-3}, and D_{6-5}, we hypothesize that control behavior changes in conditions where the forcing functions' spectral shape, bandwidth, and signal power are all equal.

b) In the second step, using forcing functions C_{8-3} and D_{6-5}, we hypothesize that behavior also changes in conditions where not only the forcing functions' spectral shape, bandwidth, and signal power are equal, but also the variance of their first derivatives.

c) In the third and final step, using the two forcing function groups, B_{7-3} vs E_{7-3} and F_{8-2} vs G_{8-2}, we hypothesize that since these forcing function groups have equal variance of the first five derivatives (including the signal itself), operator control behavior will be the same. Note that the second group represents a condition in which crossover regression effects are expected to occur.

In the next two sections the experimental results will be presented and discussed in the same sequence as the hypotheses have been introduced.

V. Results

The statistical significance of the effect of the forcing functions on the dependent measures was determined using a repeated-measures analysis of variance (ANOVA). According to Field [25], an ANOVA is allowed when the measured data complies with four properties: 1) normality, 2) homogeneity of variance, 3) sphericity, and 4) interval-scale. Because only one group of subjects was considered, the assumption of homogeneity of variance was always met. It has been indicated when the normality or sphericity assumptions were not met. When the sphericity assumption was violated, the conservative Greenhouse–Geisser [26] correction is applied.

A. Effect of Phases

1. Operator Performance and Control Behavior

To test the effect of the forcing function phases, four forcing functions with different phases ($A1_{6-4}$–$A4_{6-4}$) were used. The effects of the different phases on the normalized mean-squared error, the mean-squared control deflection, and the crossover frequency are shown in Fig. 16. A one-way repeated-measures ANOVA was applied to these dependent measures, and the results are listed in Table 9.

Figure 16 shows that the normalized mean-squared error and the mean-squared control deflection were very similar for all phase sets. The same holds for all of the frequency-domain variables, like the crossover frequency, phase margin, and precision model parameters (not shown).

The repeated-measures ANOVA confirms that the small differences observed in Fig. 16 are indeed not statistically significant, and consequently hypothesis 1 cannot be accepted.

2. Discussion

At first it seems somewhat surprising that no significant effects of the forcing function component phase were observed, since participants in previous experiments had reported these. The main difference between the previous and current experiment were the controlled element and the display type. In the previous experiments second-order aircraft dynamics were used instead of a second-order integrator. Moreover, the participants were controlling the tracking error using a pursuit display, showing both the own state and the tracking error in contrast to a compensatory display, which only shows the tracking error.

It is assumed that the use of a pursuit display results in a different control behavior in comparison to a compensatory display, since a pursuit display allows observing the forcing function directly (in contrast to observing only the error). This feedforward information enables anticipating the error signal. When a participant uses the feedforward information, he can develop a strategy avoiding

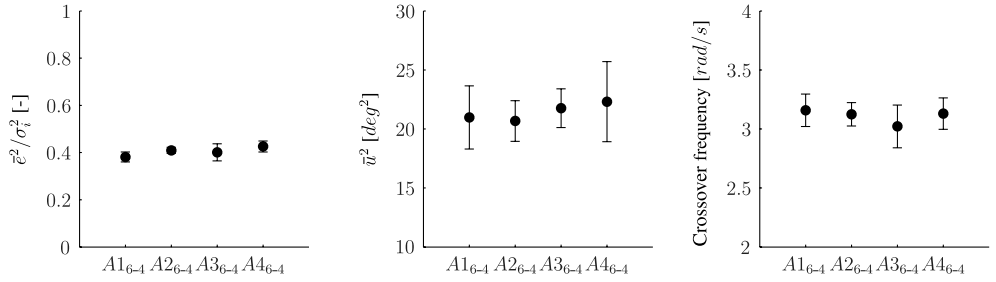

a) Normalized mean-squared error **b) Mean-squared control deflection** **c) Crossover frequency**

Fig. 16 Means and 95% confidence intervals, corrected for between-subject variability.

Table 9 Results of repeated-measures ANOVA on sinusoids components' phase

Independent variables	Dependent measures					
	Time-domain performance				Frequency-domain behavior	
	$\bar{e}^2/\sigma_i^2$		$\bar{u}^2$		ω_c	
Phase distribution	$F(3, 12)$	Sig.	$F(3, 12)$	Sig.	$F(3, 12)$	Sig.
	2.085[a]	——	0.829[a]	——	1.332[a]	——

[a]Not significant ($p \geq 0.05$).

overshooting the tracking signal. In such a case, the success rate of the strategy can become dependent on the phase of the forcing function components.

In conclusion, our first main hypothesis stating that the phases affect operator performance and control behavior cannot be accepted, and supports the opposite, i.e., that the phase can be selected freely.

In view of the different perception of the forcing function when a pursuit display is applied, it is recommended to repeat the experiment with a pursuit display to investigate the effects of the forcing function phases in a pursuit configuration.

B. Effects of Bandwidth and First Derivative Variance

First, the results for conditions B_{7-3}, C_{8-3}, and D_{6-5} will be discussed. These forcing functions had the same spectral shape, bandwidth (2.5 rad/s), and power. By considering these three conditions, we can check the validity of hypothesis 2.a using a one-way repeated-measures ANOVA.

Furthermore, the last two forcing functions also had equal variance of their first derivative (C_{8-3}: 0.728 inch^2/s^2 and D_{6-5}: 0.725 inch^2/s^2), which is approximately 60% higher than the baseline condition B_{7-3} (0.457 inch^2/s^2). To determine the effect of the first variance on the control behavior, repeated contrasts [27] were used to compare the dependent measures resulting from these two forcing functions (hypothesis 2.b).

1. *Operator Performance and Control Behavior*

The means and the 95% confidence intervals, adjusted for between-subject variability [25], of operator performance and control behavior metrics are presented in Fig. 17. The results of the main ANOVA and the repeated contrasts are summarized in Table 10.

Figure 17a shows that the normalized mean-squared error increases; hence, the performance decreases when additional sinusoids are added, especially for the high-frequency sinusoid additions in D_{6-5}. The mean-squared control activity, however, remains the same for all three conditions (Fig. 17b), and no significant effects were found.

The crossover frequency and phase margin (Figs. 17c and 17d) remain approximately the same when adding two additional sinusoids just below the forcing function bandwidth, i.e., comparing conditions B_{7-3} and C_{8-3}. Adding the two sinusoids at higher frequencies results in a significant decrease of the crossover frequency, while the phase margin remains the same. In general, the phase margin remains the same for all three conditions.

When comparing the current data with those obtained in the original experiment by McRuer et al. [2] (Fig. 17), our results appear to deviate from the STI experiment (only data from condition B_{7-3} can be compared).

In our experiment, the same control activity, a smaller error, a higher crossover frequency, and a smaller phase margin were achieved. This indicates that the participants in our experiment tried as hard (same control activity), but the smaller phase margin and higher crossover frequency indicate that they were more successful in reducing the error. This might have a number of reasons.

First, our subjects were carefully selected based on their excellent tracking skills. Contrary to the original experiment it was not a concern whether they had any aircraft piloting experience. Hence, as a group they might have performed better than the participants in the McRuer et al. [2] experiment.

A second cause could stem from differences in the feel system. The original specifications of the unique inceptor in the McRuer et al. [2] experiment could not be replicated entirely by our electrohydraulic sidestick. In precision control tasks the human controller can apply muscle cocontraction to increase his neuromuscular stiffness in order to stabilize his joints. The increased mass and damping of our inceptor might have caused a similar stabilizing effect, and better performance, compared with the very light tracker used in the original experiment.

Furthermore, differences in the run-in and total measurement time might have resulted in control behavior differences. The shorter runs in our experiment might have led to less fatigue and distraction, resulting in higher performance and less time-invariant behavior.

The final reason might stem from the quality of the experimental equipment used. It is assumed that the equipment used in the present experiment caused significantly less noise in the closed-loop. This might have allowed pilots to perform their task with smaller phase margins and higher crossover frequencies.

In view of the four reasons for the observed deviations from the original experiment we are confident in having successfully replicated the original experiment.

2. *Precision Model Parameters*

The precision model parameter means and 95% confidence intervals, adjusted for between-subject variability, are shown in Fig. 18. The ANOVA results are listed in Table 11.

The operator gain, Fig. 18a, appears to decrease when sinusoidal components are added, especially for the high-frequencies addition

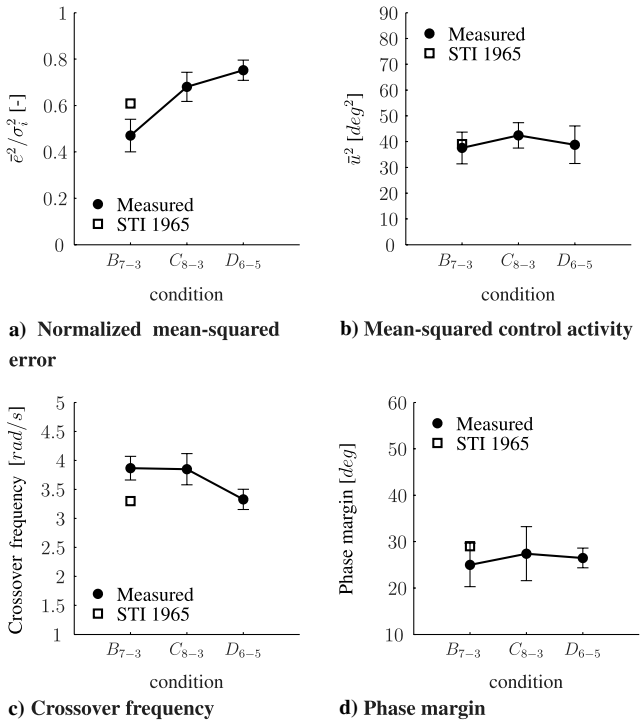

a) Normalized mean-squared error **b) Mean-squared control activity**

c) Crossover frequency **d) Phase margin**

Fig. 17 Means and 95% confidence intervals, corrected for between-subject variability.

Table 10 Results of repeated-measures ANOVA on operator performance and control behavior.

Independent variables	Dependent measures							
	Time-domain performance				Frequency-domain behavior			
	$\bar{e}^2/\sigma_i^2$		$\bar{u}^2$		ω_c		φ_M	
Same bandwidth (B_{7-3}, C_{8-5}, D_{6-5})	$F(2,8)$	Sig.	$F(2,8)$	Sig.	$F(2,8)$	Sig.	$F(2,8)$	Sig.
	22.152	[a]	0.629	[b]	7.218	[c]	0.273	[b]
Same bandwidth plus first derivative variance (C_{8-5}, D_{6-5})	$F(1,4)$	Sig.	F [d]	Sig.	$F(1,4)$	Sig.	F [d]	Sig.
	4.211	[b]	——	——	9.246	[b]	——	——

[a]Highly significant ($p < 0.01$). [b]Not significant ($p \geq 0.05$). [c]Significant ($0.01 \leq p < 0.05$). [d]Main ANOVA not significant, contrast analysis not permitted.

D_{6-5}. However, this decrease is not statistically significant. The lead-time constant, Fig. 18b, remains approximately the same between conditions B_{7-3} and C_{8-3}, but increases considerably (but not significantly) for condition D_{6-5}. The pure time delay increases slightly, when adding sinusoidal components, in particular at higher frequencies (see Fig. 18c). This increase is statistically significant.

The neuromuscular break frequency, shown in Fig. 18d, increases slightly between the baseline and C_{8-3} but then decreases significantly for the high-frequency additional sinusoidal condition D_{6-5}. The neuromuscular damping ratio, Fig. 18e, remains approximately the same, and no significant effects were found for this parameter.

Finally, note that the quality-of-fit of the linear precision model to the measured data, as indicated by the variance-accounted-for, is reasonably good with levels of 85%, but reduces considerably for condition D_{6-5}. This indicates that, for this condition, operator control behavior was more nonlinear.

3. *Discussion*

It was shown that operator performance and control behavior changed, in many cases significantly, when considering the three conditions with equal spectral shape, equal bandwidth, and equal power.

The addition of two sinusoidal components just below the bandwidth of 2.5 rad/s (C_{8-3}) only caused small changes in operator control behavior, although performance decreased significantly. No crossover regression effects were found for this condition. The crossover frequency and phase margin remained approximately constant, and so did most of the precision model parameters. The slight reduction of neuromuscular damping and the small increase in neuromuscular frequency are adaptation effects that are typical for operators that try to minimize delay in order to maintain sufficient phase margin, i.e., closed-loop stability. In this respect, our participants were trying very hard to minimize the amplification effects of their e/i characteristic (Fig. 13), especially here with the additional sinusoids. But, contrary to our expectations, these effects were minimal.

The addition of two sinusoidal components above the forcing function signal bandwidth (D_{6-5}) led to a significant degradation of operator performance, and considerable adaptation. The changes that appear, like the significantly smaller crossover frequency, the significantly larger pure time delay, and the lower gain, are typical for operators that attempt to maintain a stable control situation by reducing tracking bandwidth, at the cost of tracking performance. Since the two high-frequency components are fed through directly to the displayed error (consider the e/i transfer function of Fig. 13), it is

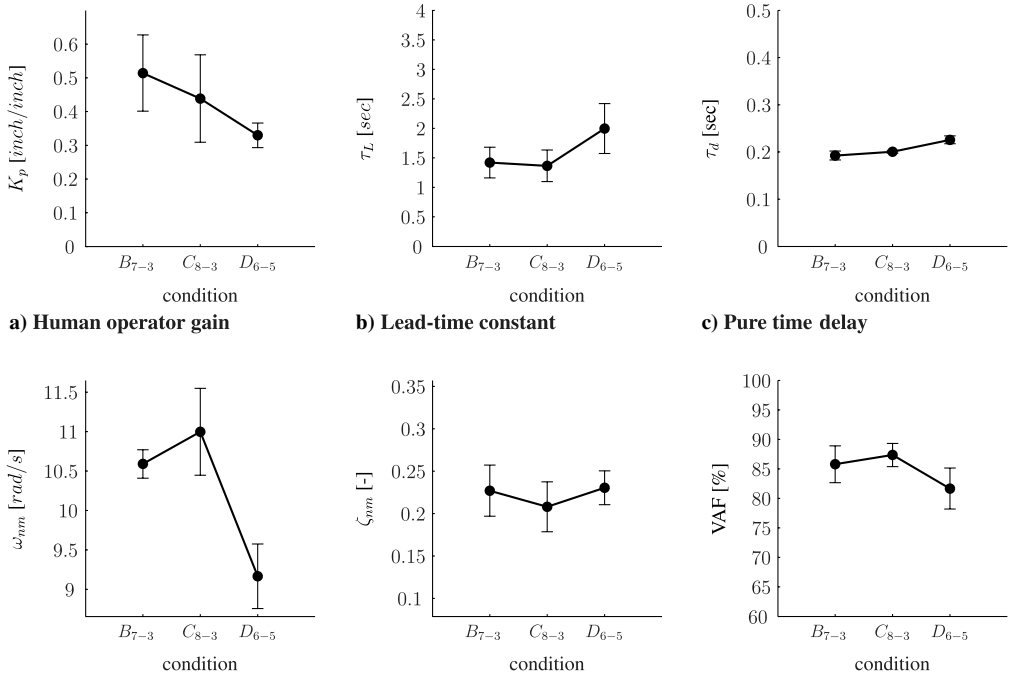

a) Human operator gain **b) Lead-time constant** **c) Pure time delay**

d) Neuromuscular break frequency **e) Neuromuscular damping** **f) Variance accounted for**

Fig. 18 Means and 95% confidence intervals, corrected for between-subject variability.

Table 11 Results of repeated-measures ANOVA on precision model parameters

Independent variables	Dependent measures									
	K_p		τ_L		τ_d		ω_{nm}		ζ_{nm}	
Same bandwidth (B_{7-3}, C_{8-5}, D_{6-5})	$F(2,8)$ 3.108	Sig. [a]	$F(2,8)$ 4.308	Sig. [a]	$F(2,8)$ 20.232	Sig. [b]	$F(1.07,4.28)$ [c] 20.534	Sig. [b]	$F(2,8)$ 0.749	Sig. [a]
Same bandwidth plus first derivative variance (C_{8-5}, D_{6-5})	F [d] ——	Sig. ——	F [d] ——	Sig. ——	$F(1,4)$ 54.510	Sig. [b]	$F(1,4)$ 20.635	Sig. [e]	F [d] ——	Sig. ——

[a]Not significant ($p \geq 0.05$). [b]Highly significant ($p < 0.01$). [c]Sphericity assumption not met, Greenhouse–Geisser correction applied. [d]Main ANOVA not significant, contrast analysis not permitted. [e]Significant ($0.01 \leq p < 0.05$).

assumed that the fluctuating error signal makes it much harder for the operators to generate the lead necessary to stabilize the double-integrator dynamics. Visual differentiation (i.e., perceiving the velocity of the error symbol) is impaired, and the operator adapts accordingly.

Summarizing, it is concluded that forcing functions that have the same spectral shape, power, bandwidth, and even equal variance of the first derivative can still lead to significantly different operator control behavior and produce varying performance. Therefore, hypotheses 2.a and 2.b cannot be rejected.

C. Effects of Variances with Different Power Spectra

To test hypothesis 2.c, which states that operator control will be equal when the variances of the forcing function's derivatives are equal, two pairs of forcing functions were evaluated in control tasks: continuous-spectrum forcing functions (B_{7-3} and F_{8-2}) are compared with sum-of-sines signals (E_{7-3} and G_{8-2}). The results have been analyzed using a two-way repeated-measures ANOVA, in which the independent variables are the forcing function shape (continuous spectrum vs sum of sines) and bandwidth (2.5 rad/s and 4.0 rad/).

1. Operator Performance and Control Behavior

Performance and control behavior means and 95% confidence intervals, all adjusted for between-subject variability, are shown in Fig. 19. The ANOVA results are summarized in Table 12.

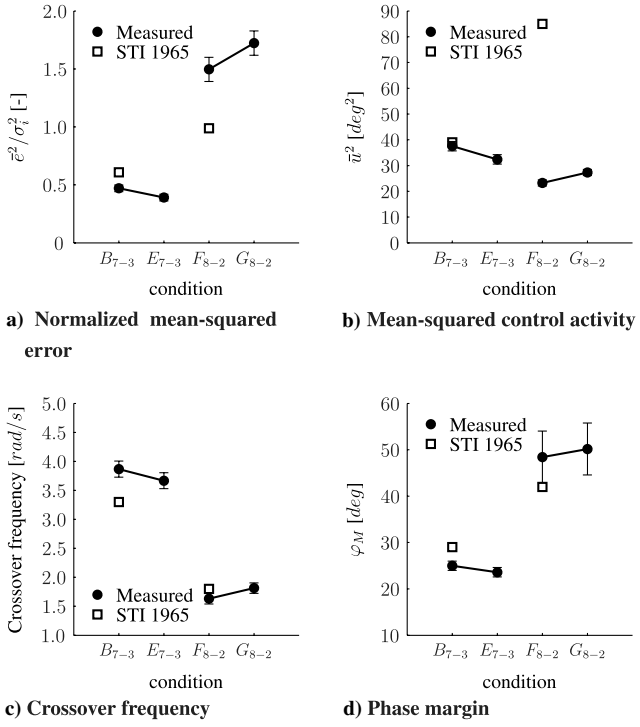

Fig. 19 Means and 95% confidence intervals, corrected for between-subject variability.

Examination of Fig. 19 reveals that small differences can be observed between the sum-of-sines and continuous-spectrum conditions. However, these small differences are not statistically significant.

For instance, when comparing B_{7-3}, the discrete spectrum, to its continuous counterpart E_{7-3}, the performance increase is accompanied by a lower control activity, a lower crossover frequency, and a lower phase margin. These spectra had a bandwidth of 2.5 rad/s, and the operator did not show crossover regression.

When comparing F_{8-2}, the discrete spectrum, to its continuous counterpart G_{8-2}, the opposite is found. The performance decrease is accompanied by a higher control activity, higher crossover frequency, and higher phase margin. These spectra had 4.0 rad/s bandwidth, and the operator showed crossover regression in both cases.

The effect of the forcing function bandwidth was highly significant in case of the NMSE, crossover frequency, and phase margin. This effect is mainly the result of the occurrence of crossover regression.

Comparing the current data with those obtained in the original experiment by McRuer et al. [2], Fig. 19 shows that our data are again similar (only conditions B_{7-3} and F_{8-2} can be compared). It was already concluded in the previous subsection that in the 2.5 rad/s bandwidth condition B_{7-3} the differences were small. When considering the data for the 4.0 rad/s bandwidth condition F_{8-2}, the differences in the frequency-domain variables are negligible, but the difference in performance and control behavior are considerable. Note, however, that here the operators have regressed their crossover frequency, and in these conditions human behavior and performance is known to be much more variable [14].

2. Precision Model Parameters

The precision model parameter means and 95% confidence intervals, adjusted for between-subject variability, are shown in Fig. 20. The significance of the effects of the forcing function shape (sum-of-sines vs continuous-spectrum, with equal first five variances) and bandwidth is listed in Table 13.

Figure 20 shows that in general the differences in the precision model parameters between the sum-of-sines and continuous-spectrum forcing functions are small. According to Table 13 none of the parameters changed significantly, which indicates that equal control behavior was achieved, even though different spectra were used. It appears that using equal variances indeed results in equal control behavior.

The only parameter that changed significantly as a result of the change in bandwidth in Table 13 is the gain K_p. This matches our expectations since the controlled element, a double integrator, only requires a change in crossover frequency to account for a change in forcing function bandwidth.

3. Discussion

Whereas control behavior, expressed by crossover frequency and phase margin, remained more or less the same, larger (but non-significant) differences were observed in the normalized mean-squared error and control activity. The applied precision model is only able to capture the linear part of human behavior, and what

Table 12 Results of repeated-measures ANOVA on performance and control behavior.

Independent variables	Dependent measures							
	Time-domain performance				Frequency-domain behavior			
	$\bar{e}^2/\sigma_i^2$		$\bar{u}^2$		ω_c		φ_M	
Spectrum type	$F(1,4)$ 4.514	Sig. [a]	$F(1,4)$ 0.257	Sig. [a]	$F(1,4)$ 0.021	Sig. [a]	$F(1,4)$ 0.987	Sig. [a]
Bandwidth	$F(1,4)$ 64.502	Sig. [b]	$F(1,4)$ 2.585	Sig. [a]	$F(1,4)$ 39.353	Sig. [b]	$F(1,4)$ 187.994	Sig. [b]

[a]Not significant ($p \geq 0.05$). [b]Highly significant ($p < 0.01$).

Table 13 Results of repeated-measures ANOVA on precision model parameters.

Independent variables	Dependent measures									
	K_p		τ_L		τ_d		ω_{nm}		ζ_{nm}	
Spectrum type	$F(1,4)$ 4.438	Sig. [a]	$F(1,4)$ 0.727	Sig. [a]	$F(1,4)$ 0.520	Sig. [a]	$F(1,4)$ 0.267	Sig. [a]	$F(1,4)$ 3.444	Sig. [a]
Bandwidth	$F(1,4)$ 33.023	Sig. [b]	$F(1,4)$ 4.680	Sig. [a]	$F(1,4)$ 1.643	Sig. [a]	$F(1,4)$ 2.428	Sig. [a]	$F(1,4)$ 3.702	Sig. [a]

[a]Not significant ($p \geq 0.05$). [b]Highly significant ($p < 0.01$).

remains is remnant. This remnant, or pilot nonlinearity, might be the explanation for the differences between the time-domain metrics and the frequency-domain metrics. It is therefore recommended to evaluate the linearity of the operator's control behavior by calculating the coherence between the operator's input and output. The coherence is defined as the squared cross-spectral density divided by the product of the autospectral densities.

When considering both pairs of forcing function definitions, characterizing both the condition without crossover regression (pair B_{7-3} and E_{7-3}) as well as the condition with regression (pair F_{8-2} and G_{8-2}), significant effects due to forcing function bandwidth were observed in the normalized mean-squared error, the crossover frequency, and the phase margin, as well as in the operator gain.

Moreover, it was observed that none of the parameters showed a significant effect due to the different spectrum shapes. It appears that equal variances of the first five derivatives (including the signal itself) have resulted in equal control behavior. This was found in conditions with and without crossover regression. Consequently, the hypothesis that equal variances result in equal control behavior (hypothesis 2.c) cannot be rejected.

VI. Conclusions

This paper focused on the effects of forcing functions on the resulting pilot control behavior. The present understanding was that these effects are governed by two parameters, the bandwidth and

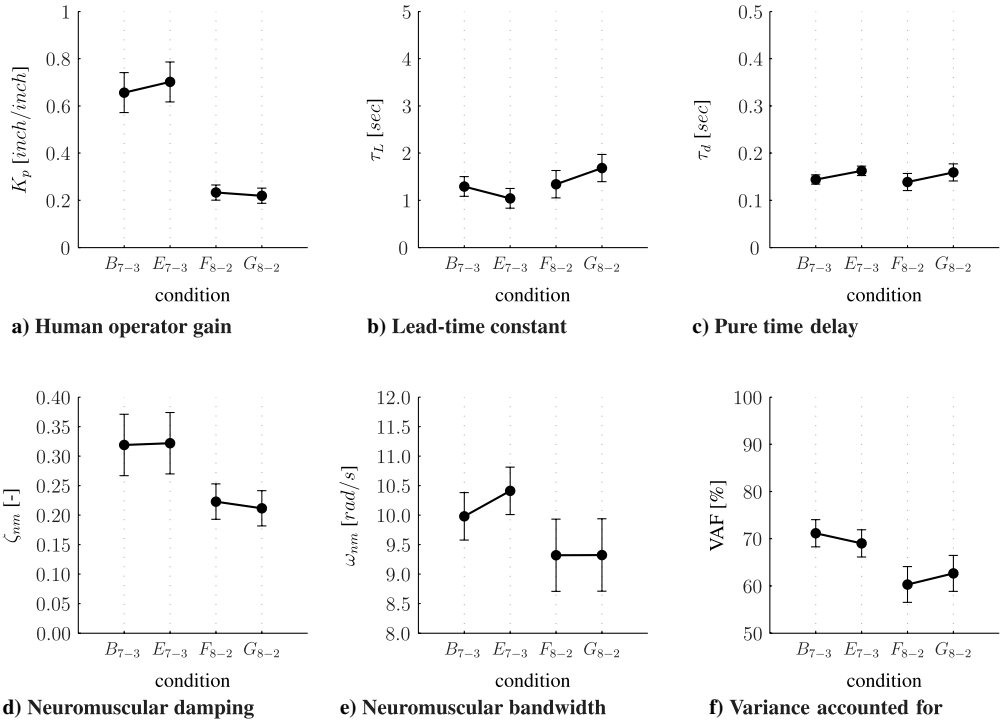

a) Human operator gain **b) Lead-time constant** **c) Pure time delay**

d) Neuromuscular damping **e) Neuromuscular bandwidth** **f) Variance accounted for**

Fig. 20 Means and 95% confidence intervals, corrected for between-subject variability.

power. Result from other studies indicated that power and bandwidth are not sufficient, and that other forcing function design parameters need to be considered as well. A theoretical analysis showed that a sum-of-sinusoids forcing function is fully defined by the phases of the sinusoids and the variance of the signal and its derivatives. For this reason the effects of the phases and the variance of the forcing function and its derivatives were investigated in this paper, and it was hypothesized that two forcing functions will lead to equal control behavior when the forcing functions have equal variance and variance of their derivatives, independent of other spectral characteristics such as bandwidth or spectral shape.

An experiment, similar to the one carried out by McRuer et al. [2], was designed to investigate the effects of the phases and the variance of the forcing function and its derivatives. The experiment consisted of a compensatory target-tracking task using second-order integrator dynamics with varying forcing function characteristics. Two main hypotheses were tested.

The first hypothesis, that operator control behavior will be affected by the selection of the phases of the sinusoids in the forcing function, had to be rejected since no significant differences were observed in the resulting mean-squared error, control activity, phase margin, and precision model parameters. Instead, the phases can be selected freely. Since other studies, using a pursuit display, unofficially did report some effects of the phases, the conclusion that the phases do not influence control behavior should be limited to compensatory situations.

The second hypothesis was that operator control behavior with different forcing functions will only be the same if the variance of the forcing function and its derivatives are the same. This hypothesis was tested in three steps. In the first step, it was tested whether the control behavior is invariant when forcing functions are used with different power spectra, but with equal the spectral shape, bandwidth, and signal power. It could be concluded that such forcing functions indeed can lead to significant differences in operator behavior and produce varying performance.

In the second step, we hypothesized that the control behavior changes in conditions where not only the forcing function's spectral shape, bandwidth, and power were equal, but also the variance of the first derivative. A contrast analysis of the results revealed that the crossover frequency was significantly different for the applied forcing functions. Consequently, specifying spectral shape, bandwidth, power, and the variance of the first derivative does not warrant equal behavior.

In the final step, the variance of the forcing function and its first four derivatives were kept the same, while the spectral shape and bandwidth were varied. The experiment results did not show any significant differences in any of the control behavior parameters. This result was found in conditions without and with crossover regression. For this reason, the hypothesis that equal variances result in equal control behavior could not be rejected and all results support its validity.

In conclusion, the study has demonstrated some limitations on the usage of bandwidth and power as the sole parameters describing the effects of a forcing function on the control behavior. Instead, when experiments with different forcing function must compared, it is advised to design the forcing functions using equal variances of signal and its derivatives.

References

[1] Elkind, J. I., *Characteristics of Simple Manual Control Systems*, Ph.D. Thesis, Lincoln Lab., Massachusetts Inst. of Technology, Cambridge, MA, 1956.

[2] McRuer, D. T., Graham, D., Krendel, E. S., and Reisener, W., Jr., "Human Pilot Dynamics in Compensatory Systems. Theory, Models, and Experiments with Controlled Element and Forcing Function Variations," Air Force Flight Dynamics Laboratory, TR AFFDL-TR-65-15, Wright–Patterson AFB, OH, 1965.

[3] Van Paassen, M. M., and Mulder, M., "Identification of Human Control Behavior," *International Encyclopedia of Ergonomics and Human Factors*, 2nd ed., edited by W. Karwowski, Taylor and Francis, London, 2006, pp. 400–407.

[4] De Jong, J. N. M., and Van Lunteren, A., "Human Operator Remnant in a Subcritical Task," *Proceedings of the Eighth Annual Conference on Manual Control*, NASA, 1972, pp. 1–2.

[5] Pool, D. M., Mulder, M., Van Paassen, M. M., and Van der Vaart, J. C., "Effects of Peripheral Visual and Physical Motion Cues in Roll-Axis Tracking Tasks," *Journal of Guidance, Control, and Dynamics*, Vol. 31, No. 6, 2008, pp. 1608–1622. doi:10.2514/1.36334

[6] Groot, T., Damveld, H. J., Mulder, M., and Van Paassen, M. M., "Effects of Aeroelasticity on the Pilot's Psychomotor Behavior," *AIAA Atmospheric Flight Mechanics Conference*, AIAA Paper No. 2006-6494, Keystone, CO, 21–24 Aug. 2006.

[7] Wasicko, R. J., McRuer, D. T., and Magdaleno, R. E., "Human Pilot Dynamics Response in Single-Loop Systems with Compensatory and Pursuit Displays," Air Force Flight Dynamics Laboratory, TR-66-137, Wright–Patterson AFB, OH, 1966.

[8] Gordon-Smith, M., "An Investigation into Certain Aspects of the Describing Function of a Human Operator Controlling a System of One Degree of Freedom," Institute of Aerospace Studies, TR 149, Univ. of Toronto, Toronto, 1970.

[9] Van der Vaart, J. C., "Modelling of Perception and Action in Compensatory Manual Control Tasks," Ph.D. Dissertation, Faculty of Aerospace Engineering, Delft Univ. of Technology, Delft, The Netherlands, Dec. 1992.

[10] Hosman, R. J. A. W., "Pilot's Perception and Control of Aircraft Motions," Ph.D. Dissertation, Faculty of Aerospace Engineering, Delft Univ. of Technology, Delft, The Netherlands, Nov. 1996.

[11] Mulder, M., and Mulder, J. A., "A Cybernetic Analysis of Perspective Flight-Path Display Dimensions," *Journal of Guidance, Control, and Dynamics*, Vol. 28, No. 3, 2005, pp. 398–411. doi:10.2514/1.6646

[12] Mulder, M., Abbink, D. A., Van Paassen, M. M., and Mulder, M., "Haptic Gas Pedal Feedback," *Ergonomics*, Vol. 51, No. 11, 2008, pp. 1710–1720. doi:10.1080/00140130802331583

[13] Damveld, H. J., "A Cybernetic Approach to Assess the Longitudinal Handling Qualities of Aeroelastic Aircraft," Ph.D. Thesis, Faculty of Aerospace Engineering, Delft Univ. of Technology, Delft, The Netherlands, May 2009.

[14] Beerens, G. C., Damveld, H. J., Mulder, M., Van Paassen, M. M., and Van Der Vaart, J. C., "Investigation into Crossover Regression in Compensatory Manual Tracking Tasks," *Journal of Guidance, Control, and Dynamics*, Vol. 32, No. 5, Sep. 2009, pp. 1429–1445. doi:10.2514/1.43528

[15] Löhner, C., Mulder, M., and Van Paassen, M. M., "Multi-Loop Identification and Modeling of Pilot's Use of Central Visual and Vestibular Motion Cues," *AIAA Modeling and Simulation Technologies Conference*, AIAA Paper No. 2005-6503, San Francisco, CA, 15–18 Aug. 2005.

[16] Nieuwenhuizen, F. M., Zaal, P. M. T., Mulder, M., Van Paassen, M. M., and Mulder, J. A., "Modeling Human Multi-Channel Perception and Control Using Linear Time-Invariant Models," *Journal of Guidance, Control, and Dynamics*, Vol. 31, No. 4, 2008, pp. 999–1013. doi:10.2514/1.32307

[17] Zaal, P. M. T., Mulder, M., Van Paassen, M. M., and Mulder, J. A., "Maximum Likelihood Estimation of Multi-Modal Pilot Control, Behavior in a Target-Following Task," *Proceedings of the IEEE Conference on Systems, Man, and Cybernetics*, Inst. of Electrical and Electronics Engineers, Piscataway, NJ, 12–15 Oct. 2008, pp. 1085–1090.

[18] McRuer, D. T., and Jex, H. R., "A Review of Quasi-Linear Pilots Models," *IEEE Transactions on Human Factors in Electronics*, Vol. HFE-8, No. 3, 1967, pp. 231–249. doi:10.1109/THFE.1967.234304

[19] McRuer, D. T., and Krendel, E. S., "Mathematical Models of Human Pilot Behavior," Systems Technology TR STI-P-146, 1974.

[20] Johnston, D. E., and Aponso, B. L., "Design Considerations of Manipulator and Feel System Characteristics in Roll Tracking," Systems Technology, NASA CR 4111, 1988.

[21] Schoukens, J., "Modelling and Identification of Linear and Nonlinear Systems," Lecture Slides, Vrije Universiteit Brussel, Brussels, 2007, pp. 1–60.

[22] Lindquist, E. F., *The Design and Analysis of Experiments in Education and Psychology*, Houghton Mifflin, Boston, 1953, p. 40.

[23] Damveld, H. J., Abbink, D. A., Mulder, M., Mulder, M., Van Paassen, M. M., Van der Helm, F. C. T., and Hosman, R. J. A. W., "Measuring the Contribution of the Neuromuscular System During a Pitch Control Task," *AIAA Modeling and Simulation Technologies Conference*, AIAA Paper No. 2009-5824, Chicago, IL, 10–13 Aug. 2009.

[24] Mulder, M., Kaljouw, W. J., and Van Paassen, M. M., "Parameterized Multi-Loop Model of Pilot's Use of Central and Peripheral Visual Motion Cues," *AIAA Modeling and Simulation Technologies Conference*, AIAA Paper No. 2005-5894, San Francisco, CA, 15–18 Aug. 2005.

[25] Field, A., *Discovering Statistics Using SPSS, ISM Introducing Statistical Methods*, 2nd ed., SAGE Publications, London, 2005.

[26] Greenhouse, S. W., and Geisser, S., "On Methods in the Analysis of Profile Data," *Psychometricka*, Vol. 24, No. 2, 1959, pp. 95–112.

[27] Serlin, R. C., and Levin, J. R., "Teaching How to Derive Directly Interpretable Coding Schemes for Multiple Regression Analysis," *Journal of Educational and Behavioral Statistics*, Vol. 10, No. 3, 1985, pp. 223–238.